Viral antigen density and confinement time regulate the reactivity pattern of CD4 T-cell responses to vaccinia virus infection

Vijay Vanguri[a], Christopher C. Govern[b], Rebecca Smith[a], and Eric S. Huseby[a,1]

[a]Department of Pathology, University of Massachusetts Medical School, Worcester, MA 01655; and [b]Department of Systems Biophysics, Foundation for Fundamental Research on Matter (FOM), Institute for Atomic and Molecular Physics (AMOLF), 1098 XG Amsterdam, The Netherlands

Edited by Bernard Malissen, Centre d'Immunologie de Marseille-Luminy, Marseille Cedex 9, France, and accepted by the Editorial Board November 16, 2012 (received for review May 16, 2012)

T-cell recognition of ligands is polyspecific. This translates into antiviral T-cell responses having a range of potency and specificity for viral ligands. How these ligand recognition patterns are established is not fully understood. Here, we show that an activation threshold regulates whether robust CD4 T-cell activation occurs following viral infection. The activation threshold was variable because of its dependence on the density of the viral peptide (p)MHC displayed on infected cells. Furthermore, the activation threshold was not observed to be a specific equilibrium affinity (K_D) or half-life ($t_{1/2}$) of the TCR–viral pMHC interaction, rather it correlated with the confinement time of TCR–pMHC interactions, i.e., the half-life ($t_{1/2}$) of the interaction accounting for the effects of TCR–pMHC rebinding. One effect of a variable activation threshold is to allow high-density viral pMHC ligands to expand CD4 T cells with a variety of potency and peptide cross-reactivity patterns for the viral pMHC ligand, some of which are only poorly activated by infections that produce a lower density of the viral pMHC ligand. These results argue that antigen concentration is a key component in determining the pattern of K_D, $t_{1/2}$ and peptide cross-reactivity of the TCRs expressed on CD4 T cells responding to infection.

kinetic proofreading T cell receptor

Upon infection, CD4 T cells scan antigen-presenting cells (APCs) for pathogen-derived peptides displayed on host MHC class II proteins (pMHCII). If a T-cell–APC encounter results in intracellular signals that exceed a threshold, naïve CD4 T cells are triggered to undergo clonal expansion and acquire effector cell functions that help eliminate pathogens (1). Thymic selection equips mature CD4 T cells with T-cell receptors (TCRs) that preferentially react with specific foreign antigens bound to MHCII molecules (2). Despite the focusing of CD4 T-cell reactivity toward unique ligands, mature CD4 T cells are polyspecific, capable of being activated by multiple, distinct pMHCII ligands (3, 4). T-cell polyreactivity can have both beneficial and detrimental effects during antiviral responses and may allow pathogen-derived peptides to activate autoimmune disease-inducing T cells (5–7). Thus, understanding how T-cell reactivity patterns develop has clear implications for vaccine strategies, as well as for understanding the origins of some immune and autoimmune-mediated diseases.

The biophysical parameters of TCR–pMHC interactions that regulate T-cell activation have been studied in vitro and in vivo (1, 8, 9). Two mechanisms allow pMHC ligands to have a stronger or weaker potency to induce T-cell activation. First, different peptides may have an enhanced or diminished ability to be processed, loaded onto to MHC, and presented on the surface of APC. This can result in peptides derived from the same protein being displayed at up to 250-fold different densities (10). Second, pMHC complexes may engage a TCR with different equilibrium affinities (K_D) or binding kinetics. T cells expressing TCRs with a weaker K_D or shorter half-life ($t_{1/2}$) for the pMHC complex usually require a higher density of ligand to be activated than do T cells expressing TCRs with a stronger K_D or longer $t_{1/2}$ (1, 8, 11–19). We and others have also suggested, based on in vitro assays, that TCR–pMHC interactions with fast on-rates (k_{on}) can have enhanced ligand potency because of the phenomenon of TCR–pMHC rebinding, the ability of a single TCR and pMHC complex to have multiple productive-binding events before diffusing away from each other (20, 21). The probability with which TCR–pMHC rebinding occurs is dependent on the k_{on} of the interaction, with a single rebinding event having the effect of doubling the dwell time of an individual TCR–pMHC interaction. The TCR–pMHC confinement-time model suggests ligand potency is dependent upon an aggregation of half-lives (t_a), taking into account the probability rebinding will occur. Whether the confinement-time model predicts the clonal expansion of T cells in vivo has not been tested.

The goal of the studies here was to identify factors that regulate antiviral CD4 T cells responses. We observed that a T-cell activation threshold determines whether robust antiviral CD4 T-cell expansion occurs. The threshold value was not set by a specific equilibrium affinity (K_D) or half-life ($t_{1/2}$) of TCR–viral pMHC interaction. Rather, it was dependent upon the density of the viral pMHC displayed on infected cells and correlated with the confinement time of TCR–pMHC interactions. One consequence of a variable activation threshold is that viral pMHC presented at a high density can robustly expand CD4 T cells with a variety of potency and peptide cross-reactivity patterns, some of which are very poorly represented in CD4 T-cell responses that are activated by the same viral pMHC presented at a lower density. These studies demonstrate that the density with which a viral pMHC is displayed can influence the pattern of K_D, $t_{1/2}$, and peptide cross-reactivity of the TCR expressed on CD4 T cells responding to infection.

Results

Vaccinia Viruses Expressing Peptides Fused to IA$^b\beta$ Are Displayed on the Cell Surface of Infected APCs at a Higher Density than Peptides Fused to GFP. Pathogen challenge results in the expansion of T cells with a range of potencies and different patterns of cross-reactivity for viral epitopes (22). Because T-cell effector functions are often dependent upon ligand concentration, we hypothesized that the density in which a viral pMHC ligand is displayed will influence T-cell reactivity patterns following infection. To test this idea, we first constructed two sets of recombinant vaccinia viruses (Vac) that were expected to display, on infected APCs, different

Author contributions: V.V., C.C.G., and E.S.H. designed research; V.V., C.C.G., R.S., and E.S.H. performed research; V.V., C.C.G., and E.S.H. contributed new reagents/analytic tools; V.V., C.C.G., R.S., and E.S.H. analyzed data; and V.V., C.C.G., and E.S.H. wrote the paper.

The authors declare no conflict of interest.

This article is a PNAS Direct Submission. B.M. is a guest editor invited by the Editorial Board.

[1]To whom correspondence should be addressed. E-mail: Eric.Huseby@umassmed.edu.

This article contains supporting information online at www.pnas.org/lookup/suppl/doi:10.1073/pnas.1208328110/-/DCSupplemental.

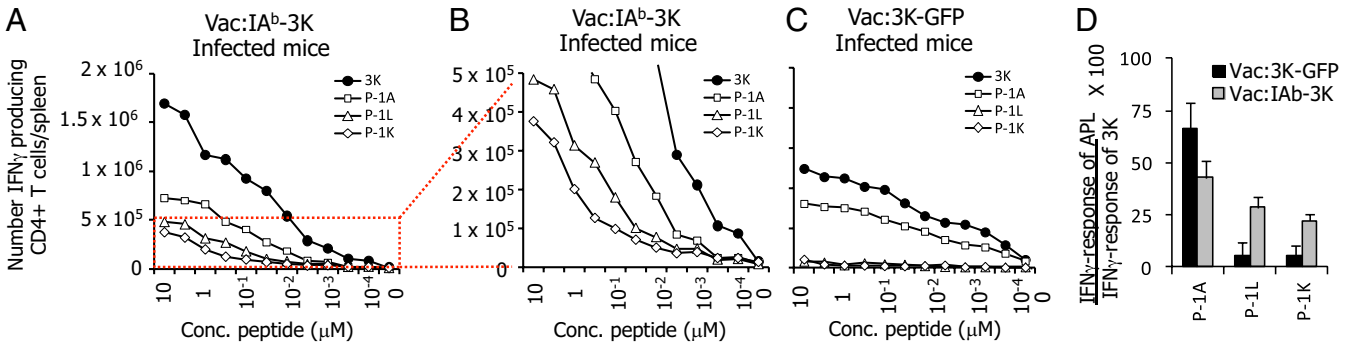

Fig. 1. Vac:IA^b–3K but not Vac:3K–GFP infection induces robust expansion of IFNγ-producing P-1L– and P-1K–reactive CD4 T cells. Mice (506β) were infected with Vac:IA^b–3K (*A* and *B*), Vac:3K–GFP (*C*), or Vac:Neg (not shown). The scale of the *y* axis is the same in both *B* and *C*. Eight days postinfection, CD4 T cells from the mice were tested for the ability to produce IFNγ in response to titrating concentrations of soluble 3K (circles), P-1A (squares), P-1L (triangles), and P-1K (diamonds). Data are the average of six total mice per group. (*D*) Comparing the size of the APL response to the 3K response in the same mouse, Vac:3K–GFP mice expanded a greater percentage of P-1A–reactive IFNγ-producing CD4 T cells ($P < 0.01$) and a lesser percentage of P-1L– and P-1K–reactive IFNγ-producing CD4 T cells ($P < 0.001$) than do mice infected with Vac:IA^b–3K.

densities of viral pMHC complexes. One set expresses the foreign antigen peptide, 3K, or 3K altered peptide ligands (APLs) (peptides derived from the wild-type peptide sequence that carry individual amino acid substitutions) fused to green fluorescent protein (GFP) (Vac:3K–GFP). The other set expresses the same 3K or APL peptides fused to the carboxyl termini of the MHCII, IA^{b}β chain (Vac:IA^b–3K) (Fig. S1 *A* and *B*). A comparison of in vitro T-cell activation experiments indicate that the 3K and 3K APL peptides are presented at approximately a 100-fold higher density on the surface of APCs infected with Vac:IA^b–peptide viruses compared with Vac:peptide–GFP viruses (see Fig. S1 and *SI Materials and Methods* for explanation of the analysis).

When C57BL/6 mice were infected with Vac:3K–GFP, a limited 3K-reactive CD4 T-cell burst size was observed, making the peptide reactivity pattern of this T-cell response difficult to quantify. To overcome this limitation, we generated mice carrying the Vβ8.1 TCRβ chain of the IA^b–3K–reactive B3K506 TCR as a transgene (506β mice). T cells in TCRβ mice express polyclonal TCRs and have been used extensively to study the dynamics of low frequency CD4 T-cell responses (23, 24).

Vac:IA^b–3K Infections Induce Robust Expansion of CD4 T Cells with Cross-Reactivity Patterns That are Poorly Represented in Mice Infected with Vac:3K–GFP. To identify peptide cross-reactivity patterns that arise in 506β mice following infections with Vac:3K–GFP and Vac:IA^b–3K, ex vivo splenocytes were challenged to produce IFNγ in response to titrating amounts of soluble 3K, or 3K APLs that carry amino acid substitutions at the P-1 residue: P-1A, P-1L, and P-1K (Fig.1 and Fig. S2). 3K APLs carrying substitutions at the P-1 residue were analyzed because this residue is a TCRα chain contact in several TCR-IA^b–3K cocrystal structures (25, 26), and 3K-reactive T cells can have different peptide fine specificities at this residue (27). Although the magnitude of response was greater in Vac:IA^b–3K–infected mice, both Vac:3K–GFP and Vac:IA^b–3K infection induced a strong IFNγ response directed at the 3K and P-1A peptides. In contrast, only Vac:IA^b–3K–infected mice had a robust IFNγ response directed at the P-1L and P-1K peptides. When the IFNγ responses directed at the P-1A, P-1L, and P-1K peptides are compared with the response to the 3K peptide in the same mouse, Vac:3K–GFP infections expand a greater frequency of CD4 T cells that react with P-1A and underproduce ones that react with P-1L and P-1K, compared with mice infected with Vac:IA^b–3K (Fig. 1*D*).

To determine whether Vac:3K–GFP infection caused 3K, P-1A, P-1L, or P-1K–reactive CD4 T cells to differentially accumulate in secondary lymphoid organs (SLO) other than the spleen, CD4 T cells from the mesenteric LN, cervical LN, bone marrow and peripheral blood were tested for the ability to be stained by IA^b tetramers. Consistently, the greatest number of 3K, P-1A, P-1L, and P-1K tetramer-reactive CD4 T cells were found in the spleen, regardless of the time point (Figs. S3 and S4). Both Vac:3K–GFP– and Vac:IA^b–3K–infected mice showed expanded populations of 3K and P-1A tetramer-reactive CD4 T cells on days 6, 8, and 28 postinfection in all SLO analyzed (Fig. 2 and Figs. S3 and S4). P-1L– and P-1K–reactive CD4 T cells were strongly expanded on days 6 and 8 postinfection with Vac:IA^b–3K, and to a lesser extent withVac:3K–GFP. At 28 d postinfection, expanded populations of P-1L– and P-1K–reactive CD4 T cells were only found in Vac:IA^b–3K–infected mice.

Vac:IA^b–3K Infections Induce Robust Activation of Medium-Potency CD4 T Cells. The findings above indicate that P-1L– and P-1K–reactive CD4 T cells are differentially expanded and maintained in 506β mice infected with Vac:IA^b–3K versus Vac:3K–GFP. We hypothesized that the high density of IA^b+3K presented on APC

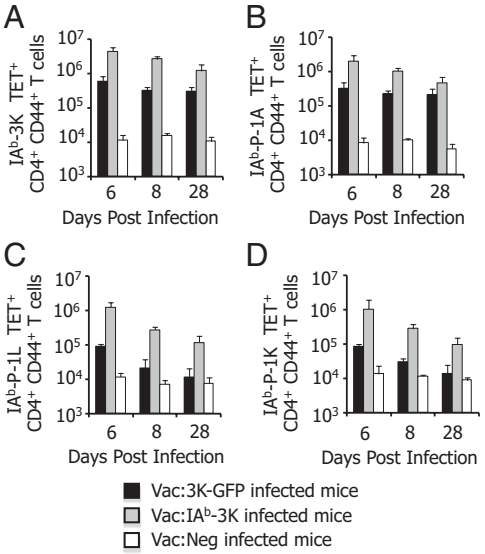

Fig. 2. CD4 T-cell populations reactive to P-1L and P-1K in 506β mice are poorly expanded and not maintained in the spleens of mice infected with Vac:3K–GFP. Mice (506β) were infected with Vac:3K–GFP (black bars), Vac:IA^b–3K (gray bars), or Vac:Neg (white bars). On days 6, 8, and 28 postinfection, 3K-reactive (*A*), P-1A–reactive (*B*), P-1L–reactive (*C*), and P-1K–reactive (*D*) CD4$^+$ CD44$^+$ T cells were quantified by staining with 1 μg/mL MHC tetramer. Data are the average of four (day 6), six (day 8), or five (day 28) total mice per group.

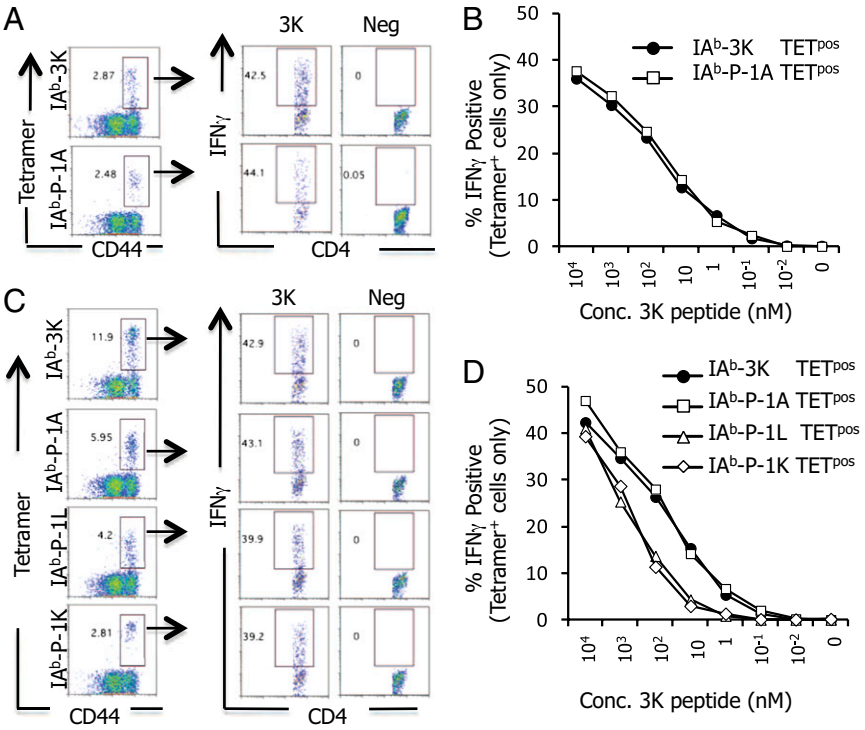

Fig. 3. Repertoire of 3K-reactive CD4 T cells that cross-react with P-1L and P-1K have a weaker potency for soluble 3K peptide than do P-1A cross-reactive CD4 T cells. (*A* and *B*) IA^b–3K and IA^b–P-1A tetramer-positive CD4 T cells from 506β mice infected with Vac:3K–GFP were analyzed for the ability to produce IFNγ in response to 1 μg/mL soluble 3K peptide (*A*) or titrating amounts of soluble 3K peptide (*B*). (*C* and *D*) IA^b–3K, –P-1A, –P-1L, and –P-1K tetramer-positive CD4 T cells from 506β mice infected with Vac:IA^b–3K were analyzed for the ability to produce IFNγ in response to 1 μg/mL soluble 3K peptide (*C*) or titrating amounts of soluble 3K peptide (*D*). Data are the average of six total mice per group.

following Vac:IA^b–3K infections was able to expand CD4 T cells with a lower potency for 3K, some of which cross-react with P-1L or P-1K. To test this idea, ex vivo IA^b–3K, –P-1A, –P-1L, and –P-1K tetramer-positive CD4 T cells were challenged to produce IFNγ in response to titrating concentrations of 3K peptide (Fig. 3). IA^b–3K and IA^b–P-1A tetramer-positive cells, isolated from either Vac:IA^b–3K– or Vac:3K–GFP–infected mice, produced IFNγ in response to similar concentrations of soluble 3K peptide (EC_{50} = 49–71 nM). In contrast, IA^b–P-1L and IA^b–P-1K tetramer-positive cells, isolated from Vac:IA^b–3K–infected mice, were ∼10-fold less sensitive to soluble 3K peptide (EC_{50} = 540–630 nM) (Fig. 3 *C* and *D* and *SI Materials and Methods*). These data indicate that the P-1L and P-1K cross-reactive CD4 T cells are medium potency subsets of the 3K response and imply that the viral pMHC density is a key component for setting the threshold that regulates robust CD4 T-cell activation.

Ligand Potency and Density Regulates the Threshold for Robust Expansion of Antiviral CD4 T Cells. To identify how the CD4 T-cell activation threshold is set, we analyzed the response of two monoclonal populations of CD4 T cells, B3K506 and B3K508, following infection in which viruses express different cross-reactive ligands. In vitro, soluble peptide versions of these ligands have different potencies to induce B3K508 and B3K506 CD4 T-cell proliferation. These potencies have been quantified based on the concentration of soluble peptide that induces half-maximal proliferation (EC_{50}) (Table S1). For the activation of naïve B3K508 T cells, the 3K peptide has a strong potency, P5R has a medium potency and P8R has a weak potency. For the activation of naïve B3K506 T cells, the 3K, P5R, and P8R peptides all have a strong potency, whereas P-1A has a medium potency (20).

Naïve B3K508 or B3K506 CD4 T cells (1×10^5) were adoptively transferred into C57BL/6 mice and then recipient mice were virally infected. Because Vac-specific CD4 T cells are enriched in the spleens of mice infected with Vac (see above), we focused our experiments on T cells resident in this organ. Vac that carry medium potency 3K APLs fused to GFP induced limited accumulation of CD4 T cells 7 d postinfection that is largely absent on day 28. This is evidenced by the B3K 508 T cells responding to Vac:P5R–GFP (Fig. 4 *A* and *B*, blue solid bar) and B3K506 T cells responding to Vac:P-1A–GFP (Fig. 4 *C* and *D*, orange solid bar). In contrast, B3K508 and B3K506 CD4 T cells responding to Vac:peptide–GFP infections carrying stronger-potency ligands (in vitro EC_{50} values 10- to 30-fold greater) induced ∼100-fold greater expansion and maintenance (Fig. 4 *A* and *B*, red solid bar; and Fig. 4 *C* and *D*, green, blue, and red solid bars).

The limited B3K508 and B3K506 T-cell response following Vac infections that carry medium potency 3K APLs fused to GFP was not attributable to ignorance of the ligand. B3K508 CD4 T cells responding to Vac:P5R–GFP infections show an intermediate expression of CD69 (18 h postinfection), CD25, and inducible T-cell costimulator (ICOS) (48 h postinfection) (Fig. S5). Three days postinfection, CD4 T cells responding to Vac:P5R–GFP infections showed modest proliferation, although they were less capable of producing IFNγ compared with CD4 T cells responding to Vac:3K–GFP infections (Fig. S5). The poor ability to make IFNγ was observed on day 7 postinfection as well, and they did not become strong producers of Th2 or Th17 cytokines (Figs. S5 and S6). B3K508 CD4 T cells responding to Vac:P8R–GFP (a weak potency peptide) also showed a clear, albeit even more limited, response at early time points postinfection.

Importantly, analysis of the other monoclonal CD4 T-cell population, B3K506 CD4 T cells, using the identical experimental setup (for which 3K, P5R, and P8R are strong potency peptides) indicates that Vac:P5R–GFP and Vac:P8R–GFP infections can strongly activate CD4 T cells (Fig. 4 and Figs. S5 and S7). These data indicate that the P5R and P8R peptides are sufficiently presented following infections to drive a robust CD4 T-cell response, demonstrating that there is nothing defective with the Vac:P5R–GFP and Vac:P8R–GFP viruses. Similar to the B3K508 CD4 T cells responding to Vac:P5R–GFP infections, an intermediate activation profile was found for B3K506 CD4 T cells responding to Vac expressing the medium potency peptide P-1A fused to GFP (Figs. S5 and S7). Collectively, these data indicate that CD4 T cells responding to a low density of medium-potency ligands undergo a partial activation process that begins very early following infection.

In contrast to the limited activation induced by Vac:peptide–GFP infections, medium-potency ligands carried in Vac:IA^b–peptide viruses induced an approximate 100- to 1,000-fold greater

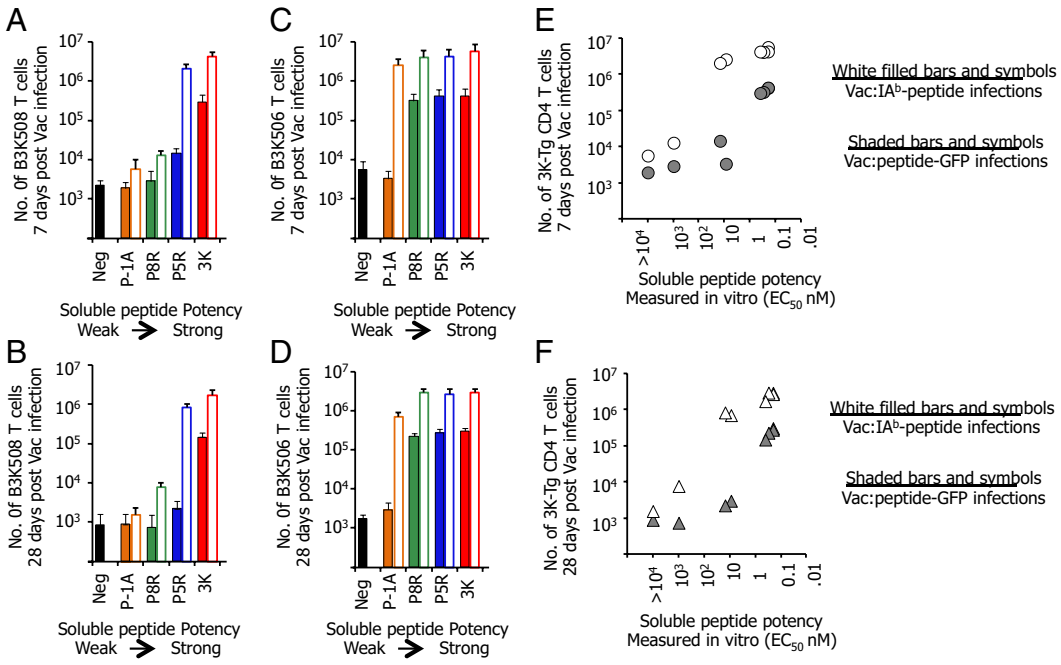

Fig. 4. Infection of mice with Vac:IA^b-linked peptides allows medium-potency ligands to induce massive CD4 T-cell expansion. A total of 1×10^5 CD45.1$^+$ B3K508 (*A* and *B*) or B3K506 (*C* and *D*) T cells were transferred into C57BL/6 mice and infected with Vac:peptide–GFP (shaded bars) or Vac:IA^b–peptide (white solid bars) viruses carrying 3K or APL peptides with different in vitro potencies. Recipient mice were analyzed on day 7 (*A* and *C*) or day 28 (*B* and *D*) postinfection for the number of B3K508 or B3K506 T cells present within the spleen. For B3K508 T cells, the 3K peptide has a strong potency, P5R has a medium potency, and P-1A and P8R have a weak potency. For B3K506 T cells, the 3K, P5, and P8R peptides all have a strong potency, whereas P-1A has a medium potency (Table S1). (*E* and *F*) Number of B3K508 and B3K506 T cells within the spleen of recipient mice on day 7 (*E*) or day 28 (*F*) postinfection with Vac:peptide–GFP (gray solid) or Vac:IA^b–peptide (white filled) plotted against the soluble peptide potency [EC_{50} (nM)]. The soluble peptide potency is quantified as the concentration of the soluble peptide that induces half-maximal proliferation (EC_{50}) of naïve CD4 T cells. Data are the average of six mice per group.

expansion (day 7) and maintenance (day 28) of naïve CD4 T cells (compare Fig. 4 *A* and *B*, empty and solid blue bars, and Fig. 4 *C* and *D*, orange bars; and Fig. S8). These robustly expanded medium potency CD4 T cells also became strong producers of TNFα and IFNγ (Fig. S9). The difference in the burst size and maintenance of CD4 T cells responding to strong potency viral ligands carried in Vac:IA^b–peptide versus Vac:peptide–GFP, however, was approximately only 10-fold (Fig. 4 *E* and *F*). These data demonstrated that a sharp threshold regulates the robust activation of antiviral CD4 T cells that is dependent upon the potency of the ligand and the density in which it is presented.

TCR–pMHC Confinement Time Predicts the in Vivo Potency of CD4 T-Cell Recognition of Viral Ligands. Models of T-cell activation suggest that the ligand potency aspect of the threshold could be set by the affinity (K_D), the half-life ($t_{1/2}$), or the confinement time (t_a) of the TCR–pMHC interaction (1, 12–21, 28). To elucidate whether these parameters correlate with the antiviral CD4 T-cell responses, we compared the number of B3K508 and B3K506 T cells expanded by each virus on days 7 or 28 postinfection with the previously measured TCR–pMHC K_D, $t_{1/2}$, or calculated t_a.

Several viral infections were identified in which neither the K_D nor the $t_{1/2}$ of the TCR–pMHC interaction predicted the size of the CD4 T-cell response (Fig. 5 *A*–*D*). For example, the B3K508 TCR has a similar K_D for IA^b+3K as does the B3K506 TCR for IA^b+P-1A (Table S1), and yet B3K508 T cells responding to Vac:3K–GFP infection expand and are maintained at ∼100-fold greater than are B3K506 T cells responding to Vac:P-1A–GFP infections (Fig. 4). Additionally, the B3K508 TCR has a similar $t_{1/2}$ when binding IA^b+P5R as does the B3K506 TCR for IA^b+3K, IA^b+P5R, and IA^b+P8R. However, B3K506 T cells responding to Vac:3K–GFP, Vac:P5R–GFP, and Vac:P8R–GFP infections expand and are maintained at a ∼30- to 100-fold greater level than are B3K508 T cells responding to Vac:P5R–GFP infections. These large differences in response are statistically significant and not likely attributable to experimental variability (two-sample t test, $P < 0.0024$ for all pairwise comparisons). In contrast, interactions with a similar calculated t_a (Table S1) (20) lead to a similar response ($P > 0.2$ for these comparisons).

To determine for the entire set of responses whether TCR–pMHC K_D, $t_{1/2}$, or calculated t_a best predicts CD4 T-cell responses in vivo, we used two additional statistical analyses. The first method used a simple linear regression to determine how strongly the response correlates with the different parameters (Fig. 5). The second analysis used a mutual information metric. This analysis looks for relationships between the dependent and independent variables without a preconceived idea of what the relationship is supposed to be, unlike linear regression, which assumes the relationship is linear (see *SI Materials and Methods* for the complete analysis). For example, it would also allow for an increased t_a to be toxic to the response past a certain threshold. However, the main motivation for using it was that the datasets appear to be nonlinear, principally around the threshold value. Instead of using a correlation coefficient, the analysis penalizes scatter in the data by quantifying the amount of information the K_A, $t_{1/2}$, or t_a provide about the response. Using all methods, we found that the calculated t_a best predicted the day 7 and day 28 response of B3K508 and B3K506 T cells responding to Vac infections, with the outlier analysis of T-cell responses grouped by a similar K_D, $t_{1/2}$, or t_a proving the most direct evidence.

Discussion

Signaling thresholds control the fate of T cells (2, 8, 9, 28, 29). Having a signaling threshold ensures that the CD4 T cells that are activated are sufficiently potent to help orchestrate pathogen clearance, while avoiding cross-reactive autoimmune responses (1, 22, 24, 30). The polyclonal T-cell repertoire that is recruited into the immune response often carries a diversity of specificities

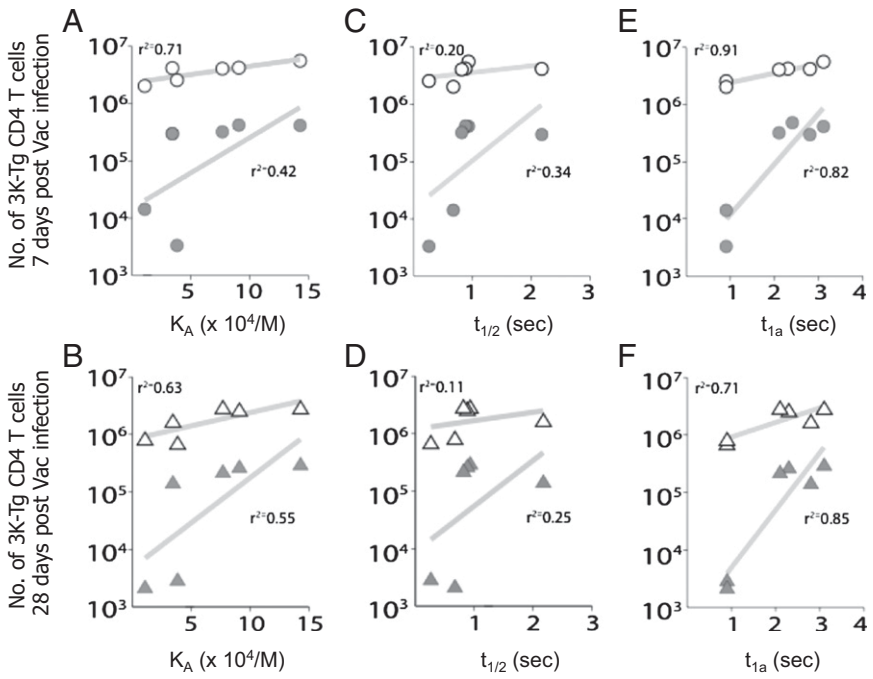

Fig. 5. TCR–pMHC confinement time predicts the burst size and maintenance of CD4 T cells responding to ligands with different equilibrium affinity or half-life. The number of B3K506 or B3K508 CD4 T cells present in the spleen on day 7 (upper row) and day 28 (lower row) following infection with Vac:peptide–GFP (gray solid) or Vac:IA^b–peptide (white filled) is shown with respect to the K_A (*A* and *B*), $t_{1/2}$ (*C* and *D*), and t_a (*E* and *F*), with the rebinding threshold set at 45,000/(M × s). Linear regression analysis indicates that the t_a of the TCR–pMHC interaction is a better predictor of burst size and maintenance than the K_A or $t_{1/2}$. r^2 values are given in each graph.

and potencies for the invading pathogens (22). How the activation threshold set point relates to the biophysics of TCR–pMHC interactions and the reactivity pattern of CD4 T cells that are recruited into antiviral immunity is less well characterized.

Polyclonal CD4 T-cell responses to vaccinia infection are sensitive to ligand density. In vitro, Vac:IA^b–3K infection resulted in a higher concentration of IA^b+3K to be presented by APCs than Vac:3K–GFP infection. In vivo, Vac:IA^b–3K infection induced a larger 3K-specific CD4 T-cell response than Vac:3K–GFP infection. Because APC presentation of pMHC in vivo has a half-life of display (31) and CD4 T-cell responses are sensitive to the duration of antigen presentation (31–34), the larger T-cell response following Vac:IA^b–3K infection may result from a longer duration of antigen presentation, as well as the higher concentration of ligand presented during T-cell priming.

Qualitative changes to the T-cell response were also observed following Vac:IA^b–3K versus Vac:3K–GFP infections. The 506β mice infected with Vac:IA^b–3K expanded a large population of IFNγ-producing CD4 T cells that recognized the 3K variant ligands, P-1L and P-1K. In contrast, Vac:3K–GFP expanded CD4 T cells with these cross-reactivities very poorly. An increased precursor frequency of CD4 T cells in 506β mice for 3K and the 3K APLs may allow these lower potency, P-1L and P-1K cross-reactive CD4 T cells to be expanded following Vac:IA^b–3K infections, whereas in a completely polyclonal population these cells would fail to be activated because of some aspect of T-cell competition (35). However, this need not be the case, because primary CD4 T-cell responses have a range of affinity, avidity or potency for the immunizing ligand (36–38). These data argue that high-density viral pMHC ligands allow CD4 T cells with lower potencies and, in some cases, different peptide cross-reactivity patterns to be recruited into the immune response.

The tight threshold that regulates whether B3K508 or B3K506 CD4 T cells undergo robust expansion is set by the potency of virally expressed peptide ligand and by the density in which it is presented. Changes in viral ligand density resulted in dramatically different CD4 T-cell responses to medium-potency ligands, indicating that the potency aspect of the threshold for robust CD4 T-cell activation is not a fixed value. This finding for vaccinia responses is similar to recent experiments showing that antigen dose and potency can regulate the transition of T-cell–APC interactions from brief serial encounters to longer, sustained interactions that allow full T-cell signaling to occur (39–42). The sharp potency threshold is also consistent with experiments suggesting an avidity threshold regulates CD4 T-cell expansion (24, 31, 43).

CD4 T cells responding to weak and medium potency viral ligands which did not pass the threshold were not ignorant as they up-regulated activation markers and underwent limited proliferation. CD4 T cells activated in vivo by low-potency ligands can differentiate into T helper 2 (Th2)-phenotype CD4 T cells (1, 44–46); however, we did not observe this differentiation pattern. This suggests that the antiviral inflammatory response can override the ability of low potency pMHC complexes to induce Th2 differentiation. On the opposite end of the spectrum, T cells responding to a high density of strong-potency ligands can have attenuated responses that skew toward being of lower avidity (18, 37, 47, 48). The magnitude of the CD4 T-cell responses studied here increased with the density and potency of the ligand displayed, indicating that the critical upper potency threshold was not surpassed even when the B3K506 CD4 T cells, which have a strong potency with IA^b+3K (in vitro EC_{50} = 200 pM), were activated following Vac:$1A^b$–3K infections.

The B3K508 and B3K506 TCRs engage the series of virally expressed pMHC ligands with different binding kinetics. This allowed us to compare how different parameters of the TCR–pMHC interaction relate to the in vivo potency of ligands. For an individual clonotype (B3K508 or B3K506 T cells), responses track with both the K_A and $t_{1/2}$. The threshold for activation following Vac:peptide–GFP infections was approximately a K_A of ~4×10^4 (K_D = ~25 μM) and $t_{1/2}$ ~0.7 s. The responses of individual T-cell clonotypes track with both the K_A and the $t_{1/2}$ because the k_{on} for each TCR binding the different 3K APLs does not significantly change. Thus, changes in the $t_{1/2}$ resulted in the commensurate change in the K_A. However, when the B3K508 and B3K506 T-cell responses were compared with each other, several outlier responses were observed with both the K_A and $t_{1/2}$. This likely results from differences in the on-rates of the B3K508 versus B3K506 TCRs for IA^b+3K and the APLs. Outlier responses were not observed when T-cell responses were compared with the confinement time (t_a). The confinement-time model predicts that the potency of a ligand can depend on both the half-life of the interaction (which controls the duration of

each individual binding event) and the equilibrium affinity of the interaction (which influences the number of rebindings before complete disengagement). For the B3K508 TCR, the on-rate is slow and t_a is determined by the half-life. For the B3K506 TCR, the on-rate is fast, rebinding can occur and t_a is a sum of $t_{1/2}$ before complete TCR–pMHC disengagement.

Recently, the 2D binding properties of TCR and pMHC have been directly measured using different techniques (49–51). In each system, both the k_{on} and k_{off} are strikingly faster than the rates measured in solution. In one report, in vitro ligand potency correlated with both k_{on} and k_{off} (50), whereas a second group found that the TCR–pMHC bond lifetime and the bond mechanical strength correlated with in vitro potency (51). Thus, there is still some discrepancy as to which 2D biophysical measurement best accounts for ligand potency. Because TCR–pMHC rebinding is proportional to k_{on}, the observation that 2D k_{on} are much faster than those measured in solution further emphasizes that TCR–pMHC rebinding can significantly contribute to ligand potency and, thus, to the reactivity pattern of antiviral CD4 T-cell responses as well.

Materials and Methods

C57BL/6 and C57BL/6.SJL mice were purchased from The Jackson Laboratory. Rag1$^{-/-}$ B3K506 and Rag1$^{-/-}$ B3K508 TCR Tg mice have been described previously (27). TCRβ Tg mice were established by expressing the rearranged B3K506 Vβ8.1 chain using the human CD2 promoter (52). All mice were maintained in a pathogen-free environment in accordance with institutional guidelines in the Animal Care Facility at the University of Massachusetts Medical School and experiments approved by the institute's Institutional Animal Care and Use committee. Peptides were purchased from the Medical Research Center at National Jewish Medical Center. The 3K peptide is FEAQKAKANKAVD, numbered P-2 to P11; the P-1A peptide is FAAQKAKANKAVD.

Additional details are provided in *SI Material and Methods*.

ACKNOWLEDGMENTS. We thank Andrew Mugler for helpful discussion on mutual information. This work was supported by Beckman Young Investigator and Searle Scholars Awards and National Institutes of Health (NIH) Grants RAI088495A and DK095077 (to E.S.H.). C.C.G. was supported by the Stichting voor Fundamenteel Onderzoek der Materie (FOM), Nederlandse Organisatie voor Wetenschappelijk Onderzoek (NWO). E.S.H. is a member of the University of Massachusetts Medical School Diabetes and Endocrinology Research Center (NIH Grant DK32520).

1. Corse E, Gottschalk RA, Allison JP (2011) Strength of TCR-peptide/MHC interactions and in vivo T cell responses. *J Immunol* 186(9):5039–5045.
2. Starr TK, Jameson SC, Hogquist KA (2003) Positive and negative selection of T cells. *Annu Rev Immunol* 21:139–176.
3. Wucherpfennig KW, et al. (2007) Polyspecificity of T cell and B cell receptor recognition. *Semin Immunol* 19(4):216–224.
4. Eisen HN, Chakraborty AK (2010) Evolving concepts of specificity in immune reactions. *Proc Natl Acad Sci USA* 107(52):22373–22380.
5. Kosmrlj A, et al. (2010) Effects of thymic selection of the T-cell repertoire on HLA class I-associated control of HIV infection. *Nature* 465(7296):350–354.
6. Welsh RM, Che JW, Brehm MA, Selin LK (2010) Heterologous immunity between viruses. *Immunol Rev* 235(1):244–266.
7. Wucherpfennig KW, Strominger JL (1995) Molecular mimicry in T cell-mediated autoimmunity: Viral peptides activate human T cell clones specific for myelin basic protein. *Cell* 80(5):695–705.
8. Davis MM, et al. (1998) Ligand recognition by alpha beta T cell receptors. *Annu Rev Immunol* 16:523–544.
9. Morris GP, Allen PM (2012) How the TCR balances sensitivity and specificity for the recognition of self and pathogens. *Nat Immunol* 13(2):121–128.
10. Velazquez C, DiPaolo R, Unanue ER (2001) Quantitation of lysozyme peptides bound to class II MHC molecules indicates very large differences in levels of presentation. *J Immunol* 166(9):5488–5494.
11. Sykulev Y, et al. (1994) Kinetics and affinity of reactions between an antigen-specific T cell receptor and peptide-MHC complexes. *Immunity* 1(1):15–22.
12. Matsui K, Boniface JJ, Steffner P, Reay PA, Davis MM (1994) Kinetics of T-cell receptor binding to peptide/I-Ek complexes: Correlation of the dissociation rate with T-cell responsiveness. *Proc Natl Acad Sci USA* 91(26):12862–12866.
13. Kersh GJ, Kersh EN, Fremont DH, Allen PM (1998) High- and low-potency ligands with similar affinities for the TCR: The importance of kinetics in TCR signaling. *Immunity* 9(6):817–826.
14. Stefanová I, et al. (2003) TCR ligand discrimination is enforced by competing ERK positive and SHP-1 negative feedback pathways. *Nat Immunol* 4(3):248–254.
15. Holler PD, Kranz DM (2003) Quantitative analysis of the contribution of TCR/pepMHC affinity and CD8 to T cell activation. *Immunity* 18(2):255–264.
16. Tian S, Maile R, Collins EJ, Frelinger JA (2007) CD8+ T cell activation is governed by TCR-peptide/MHC affinity, not dissociation rate. *J Immunol* 179(5):2952–2960.
17. McKeithan TW (1995) Kinetic proofreading in T-cell receptor signal transduction. *Proc Natl Acad Sci USA* 92(11):5042–5046.
18. Kalergis AM, et al. (2001) Efficient T cell activation requires an optimal dwell-time of interaction between the TCR and the pMHC complex. *Nat Immunol* 2(3):229–234.
19. Rosette C, et al. (2001) The impact of duration versus extent of TCR occupancy on T cell activation: A revision of the kinetic proofreading model. *Immunity* 15(1):59–70.
20. Govern CC, Paczosa MK, Chakraborty AK, Huseby ES (2010) Fast on-rates allow short dwell time ligands to activate T cells. *Proc Natl Acad Sci USA* 107(19):8724–8729.
21. Aleksic M, et al. (2010) Dependence of T cell antigen recognition on T cell receptor-peptide MHC confinement time. *Immunity* 32(2):163–174.
22. Davenport MP, Price DA, McMichael AJ (2007) The T cell repertoire in infection and vaccination: Implications for control of persistent viruses. *Curr Opin Immunol* 19(3):294–300.
23. Jorgensen JL, Esser U, Fazekas de St Groth B, Reay PA, Davis MM (1992) Mapping T-cell receptor-peptide contacts by variant peptide immunization of single-chain transgenics. *Nature* 355(6357):224–230.
24. Malherbe L, Hausl C, Teyton L, McHeyzer-Williams MG (2004) Clonal selection of helper T cells is determined by an affinity threshold with no further skewing of TCR binding properties. *Immunity* 21(5):669–679.
25. Dai S, et al. (2008) Crossreactive T Cells spotlight the germline rules for alphabeta T cell-receptor interactions with MHC molecules. *Immunity* 28(3):324–334.
26. Stadinski BD, et al. (2011) A role for differential variable gene pairing in creating T cell receptors specific for unique major histocompatibility ligands. *Immunity* 35(5):694–704.
27. Huseby ES, et al. (2005) How the T cell repertoire becomes peptide and MHC specific. *Cell* 122(2):247–260.
28. Krogsgaard M, Davis MM (2005) How T cells 'see' antigen. *Nat Immunol* 6(3):239–245.
29. Palmer E, Naeher D (2009) Affinity threshold for thymic selection through a T-cell receptor-co-receptor zipper. *Nat Rev Immunol* 9(3):207–213.
30. Messaoudi I, Guevara Patiño JA, Dyall R, LeMaoult J, Nikolich-Zugich J (2002) Direct link between mhc polymorphism, T cell avidity, and diversity in immune defense. *Science* 298(5599):1797–1800.
31. Obst R, van Santen HM, Mathis D, Benoist C (2005) Antigen persistence is required throughout the expansion phase of a CD4(+) T cell response. *J Exp Med* 201(10):1555–1565.
32. Bajénoff M, Wurtz O, Guerder S (2002) Repeated antigen exposure is necessary for the differentiation, but not the initial proliferation, of naive CD4(+) T cells. *J Immunol* 168(4):1723–1729.
33. Gett AV, Sallusto F, Lanzavecchia A, Geginat J (2003) T cell fitness determined by signal strength. *Nat Immunol* 4(4):355–360.
34. Schrum AG, Turka LA (2002) The proliferative capacity of individual naive CD4(+) T cells is amplified by prolonged T cell antigen receptor triggering. *J Exp Med* 196(6):793–803.
35. Kedl RM, Kappler JW, Marrack P (2003) Epitope dominance, competition and T cell affinity maturation. *Curr Opin Immunol* 15(1):120–127.
36. Busch DH, Pilip I, Pamer EG (1998) Evolution of a complex T cell receptor repertoire during primary and recall bacterial infection. *J Exp Med* 188(1):61–70.
37. Rees W, et al. (1999) An inverse relationship between T cell receptor affinity and antigen dose during CD4(+) T cell responses in vivo and in vitro. *Proc Natl Acad Sci USA* 96(17):9781–9786.
38. Savage PA, Boniface JJ, Davis MM (1999) A kinetic basis for T cell receptor repertoire selection during an immune response. *Immunity* 10(4):485–492.
39. Hugues S, et al. (2004) Distinct T cell dynamics in lymph nodes during the induction of tolerance and immunity. *Nat Immunol* 5(12):1235–1242.
40. Skokos D, et al. (2007) Peptide-MHC potency governs dynamic interactions between T cells and dendritic cells in lymph nodes. *Nat Immunol* 8(8):835–844.
41. Henrickson SE, et al. (2008) T cell sensing of antigen dose governs interactive behavior with dendritic cells and sets a threshold for T cell activation. *Nat Immunol* 9(3):282–291.
42. Kastenmüller W, Gerner MY, Germain RN (2010) The in situ dynamics of dendritic cell interactions. *Eur J Immunol* 40(8):2103–2106.
43. Williams MA, Ravkov EV, Bevan MJ (2008) Rapid culling of the CD4+ T cell repertoire in the transition from effector to memory. *Immunity* 28(4):533–545.
44. Constant S, Pfeiffer C, Woodard A, Pasqualini T, Bottomly K (1995) Extent of T cell receptor ligation can determine the functional differentiation of naive CD4+ T cells. *J Exp Med* 182(5):1591–1596.
45. Tao X, Grant C, Constant S, Bottomly K (1997) Induction of IL-4-producing CD4+ T cells by antigenic peptides altered for TCR binding. *J Immunol* 158(9):4237–4244.
46. Rogers PR, Croft M (1999) Peptide dose, affinity, and time of differentiation can contribute to the Th1/Th2 cytokine balance. *J Immunol* 163(3):1205–1213.
47. Wherry EJ, Puorro KA, Porgador A, Eisenlohr LC (1999) The induction of virus-specific CTL as a function of increasing epitope expression: Responses rise steadily until excessively high levels of epitope are attained. *J Immunol* 163(7):3735–3745.
48. Corse E, Gottschalk RA, Krogsgaard M, Allison JP (2010) Attenuated T cell responses to a high-potency ligand in vivo. *PLoS Biol* 8(9):8.
49. Huppa JB, et al. (2010) TCR-peptide-MHC interactions in situ show accelerated kinetics and increased affinity. *Nature* 463(7283):963–967.
50. Huang J, et al. (2010) The kinetics of two-dimensional TCR and pMHC interactions determine T-cell responsiveness. *Nature* 464(7290):932–936.
51. Robert P, et al. (2012) Kinetics and mechanics of two-dimensional interactions between T cell receptors and different activating ligands. *Biophys J* 102(2):248–257.
52. Zhumabekov T, Corbella P, Tolaini M, Kioussis D (1995) Improved version of a human CD2 minigene based vector for T cell-specific expression in transgenic mice. *J Immunol Methods* 185(1):133–140.

Supporting Information

Vanguri et al. 10.1073/pnas.1208328110

SI Materials and Methods

Virus, Tetramers, and Infections. IA^b–3K and IA^b–3K APL tetramers were constructed as described previously (1). Vac expressing $IA^b\beta$-linked peptide and peptides fused to the carboxyl termini of GFP were constructed using standard techniques. Mice were infected i.p. with 10^7 pfu of recombinant vaccinia viruses.

In Vitro T-Cell Activation and Intracellular Cytokine Production. T-cell activation in vitro was assessed by incubating 3×10^5 naïve $Rag1^{-/-}$ B3K506 or B3K508 $CD4^+$ T cells for 4 h with 1×10^5 bone marrow-derived dendritic cells (BM-DCs) infected with either Vac:IA^b–peptide or Vac:peptide–GFP viruses in the presence of GolgiStop and GolgiPlug (1 μL/mL; BD Biosciences). T cells were then surfaced stained with anti-CD4 and anti-CD8, washed, fixed in 2% (vol/vol) formaldehyde, and stained for intracellular TNFα using a Cytofix/Cytoperm kit (BD Biosciences) using the manufacturer's protocol. TNFα expression by $CD4^+$ T cells was assessed using flow cytometry (FACSCaliber; BD Biosciences) and analyzed using FlowJo Version 8.3 (TreeStar). BM-DCs were differentiated in vitro by growing BM with GM-CSF for 7 d following standard procedures. BM-DCs were then infected with Vac viruses at a multiplicity of infection (MOI) of 3 for 12 h before incubation with CD4 T cells.

To analyze CD4 T-cell responses in 506β mice following Vac infection, 5×10^6 spleen cells were pulsed with titrating concentrations of 3K or APLs in the presence of GolgiStop and GolgiPlug (1 μL/mL; BD Biosciences) for 5 h at 37 °C, then cell surfaced stained, fixed, and stained for intracellular TNFα and IFNγ expression. In some experiments, IA^b–3K, –P-1A, –P-1L, or –P-1K tetramers were added during the last 2 h of stimulation at a final concentration of 10 μg/mL.

Tetramer and Antibody Stains. Spleen cells (5×10^6) from Vac-infected mice were incubated with anti-Fc receptor antibody 2.4G2, then stained with 10 μg/mL either IA^b–3K, –P-1A, –P-1L, or –P-1K tetramer for 90 min at 37 °C. Cells were washed and stained with antibodies specific for Thy1.2, CD4, CD8, B220, and CD44. In some experiments, these cells were also stained with antibodies specific for CD69, CD25, and ICOS or analyzed for the dilution of carboxyfluorescein succinimidyl ester dye.

Adoptive-Transfer Experiments. B3K506 or B3K508 CD4 T cells (1×10^5) were transferred i.v. into congenically marked C57BL/6.SJL ($CD45.1^+$) mice. Mice were infected with 10^7 pfu vaccina virus 2 h after T-cell transfer, and the responding CD4 T cells were analyzed at 18 h, 48 h, 7 d, or 28 d postinfection.

EC_{50} Determination. Each dose–response curve was scaled such that the responses at no stimulation and 10 mm were 0 and 1, respectively, assuming saturation by 10 mM. The concentration at which the response was half-maximal (EC_{50}) was determined by linear interpolation after log-transforming the peptide concentration.

Estimating the Potency and, thus, the Relative Concentration of Viral–pMHC Complexes Displayed Following Infections. Two sets of recombinant vaccinia viruses (Vac) were constructed. One set of viruses expresses the foreign-antigen peptide, 3K, or 3K APLs (peptides derived from the wild-type peptide sequence that carry individual amino acid substitutions) fused to GFP (Vac:3K–GFP). The other set expresses the same 3K or 3K APL peptides fused to the carboxyl termini of the MHCII, $IA^b\beta$ chain (Vac:IA^b–3K) (Fig. S1 *A* and *B*). The two sets were expected to produce, on infected APCs, different densities of viral pMHC complexes. The soluble peptide versions of the 3K APL used in this study have strong, medium, and weak abilities to activate the 3K-reactive, B3K506 and B3K508 CD4 T cells (2). For example, the soluble 3K peptide has a strong potency to activate B3K506 CD4 T cells, requiring only 3 nM soluble 3K peptide loaded onto BM-DCs to induce the half-maximal amount of TNFα expression (TNFα EC_{50}). In contrast, the medium-potency 3K, P-1A APL and the weak-potency 3K, P-1K APL require 68 nM and 5,500 nM soluble peptide, respectively, to induce half-maximal TNFα expression. For the B3K508 CD4 T cells, the soluble 3K peptide has a strong potency requiring only 6 nM soluble peptide to induce half-maximal TNFα expression, whereas the medium potency 3K APL, P5R, requires 87 nM soluble peptide for a similar induction of TNFα [see table S1 by Govern et al. (2) for a complete list of APL and the EC_{50} values of TNFα expression and in vitro proliferation for naïve B3K506 and B3K508 CD4 T cells].

We observed that naïve B3K506 and B3K508 CD4 T cells always produced equal or greater amounts of TNFα in vitro when challenged with BM-DCs infected with Vac:IA^b–peptide viruses compared with BM-DCs infected with Vac:peptide–GFP viruses expressing the same 3K APL (Fig. S1 *C* and *D*). B3K506 and B3K508 CD4 T cells incubated with C57BL/6-derived, Vac:IA^b–3K– or Vac:3K–GFP–infected BM-DCs induced maximal amounts of TNFα. These data indicate that both Vac:3K–GFP– and Vac:IA^b–3K–infected BM-DCs create and present enough IA^b+3K complexes on the cell surface to fully activate the B3K506 and B3K508 CD4 T cells in this in vitro assay. In contrast, BM-DCs infected with the Vac:IA^b–peptide viruses Vac:IA^b–P-1A, Vac:IA^b–P-1K, or Vac:IA^b–P8A induce more TNFα production from B3K506 CD4 T cells than BM-DCs infected with the corresponding Vac:peptide–GFP viruses, Vac:P-1A–GFP, Vac:P-1K–GFP, or Vac:P8A–GFP (Fig. S1*C*). Similarly, Vac:IA^b–P5R– and Vac:IA^b–P8R–infected BM-DCs induce more TNFα production from B3K508 CD4 T cells compared with BM-DCs infected with the corresponding Vac:peptide–GFP viruses, Vac:P5R–GFP or Vac:P8R–GFP (Fig. S1*D*). These data indicate that BM-DCs infected with Vac:IA^b–peptide viruses create enough viral pMHC complexes displayed on the cell surface such that even weak and medium potency peptides are able to induce TNFα expression from B3K506 or B3K508 CD4 T cells. In contrast, BM-DCs infected with the matching Vac:peptide–GFP virus did not create enough viral pMHC complexes displayed on the cell surface to induce an equivalent level of TNFα expression when the peptides were of weak or medium potency.

The in vitro TNFα production assay uses purified CD4 T cells mixed with infected BM-DCs for a short incubation time (4 h), with a 3:1 ratio of CD4 T cells and BM-DCs. Thus, the assay primarily tests the ability of BM-DCs to directly present pMHC complexes at a sufficient level to activate T cells and occurs in the absence of most indirect effects on T-cell activation that can occur during in vivo immune responses that may confound the readout, such as T-cell competition or T-cell differentiation. Because in vitro T-cell activation assays are strongly sensitive to antigen concentration, the greater potency of BM-DCs infected with Vac:IA^b–P-1A, Vac:IA^b–P-1K, and Vac:IA^b–P8A versus Vac:P-1A–GFP, Vac:P-1K–GFP, and Vac:P8A–GFP to activate B3K506 CD4 T cells, for example, strongly suggests that BM-DCs infected with Vac:IA^b–peptide viruses create a higher

density of viral pMHC complexes on the cell surface compared with BM-DCs infected with Vac:peptide–GFP viruses.

We sought to estimate the difference in the potency of BM-DCs infected with Vac:IA^b–peptide versus Vac:peptide–GFP viruses and, thus, the relative concentration of viral pMHC complexes displayed following infections. A previous study determined how the T cells in our study respond to increasing concentrations of various soluble peptide ligands (2). Our current study determined how the CD4 T cells respond to BM-DCs infected with vaccinia viruses that express these same peptides. We could, therefore, estimate the concentration of soluble ligand (3K or 3K APL) required to produce the same response as BM-DCs infected with each virus; we called this the "equivalent soluble ligand concentration" for infection. To facilitate this estimation, we modeled the dose–response curves previously obtained from experiments with soluble ligand as sigmoidal curves:

$$\frac{r}{r_{\max}} = \frac{1}{1 + (c/EC_{50})^{-N}} \qquad \textbf{[S1]}$$

where r is the TNFα response to a concentration, c, of a soluble ligand. The parameters N and $r_{\max}$, assumed to be the same for all peptide-TCR interactions, describe how sensitively the response depends on the concentration and the maximal TNFα response at saturating concentrations of peptides, respectively.

We assumed that the equivalent soluble ligand concentrations are the same for all ligands introduced with either Vac:peptide–GFP infections (c_{GFP}) or Vac:IA^b–peptide infections (c_{IAb}). This assumption is consistent with previous studies that have shown several of the peptides bind IA^b within a twofold difference (3); the rest of the APLs have substitutions at the same, non-MHC anchor residues. We then used Eq. **S1** with measured TNFα responses following infection, r, and EC_{50} values fit from soluble ligand experiments for each pMHC–TCR interaction to simultaneously fit the equivalent soluble ligand concentrations, c_{GFP} and c_{IAb}, the maximal response, $r_{\max}$, and the sensitivity, N, for our experiments in this study (Fig. S1*E*).

The resulting fit parameters were $n = 1$, $r_{\max} = 60\%$, $c_{\mathrm{GFP}} = 35$ nM, and $c_{\mathrm{IAb}} = 2{,}100$ nM. Note that the fit value for N agrees well with the soluble ligand dose–response curves, a check on the model; the parameter $r_{\max}$ is expected to vary across experiments (Fig. S1*F*). The ratio of equivalent soluble ligand concentrations, $c_{\mathrm{IAb}}/c_{\mathrm{GFP}}$, is ∼100. If it is assumed that soluble peptides are loaded onto MHC molecules proportionally to their concentration in solution within the experimental concentration range, the 3K and 3K APL peptides are presented at approximately a 100-fold higher density on the surface of APCs infected with Vac:IA^b–3K, compared with Vac:3K–GFP viruses.

Why might BM-DCs infected with Vac:IA^b–peptide viruses create more viral pMHC displayed on the cell surface than those infected with Vac:peptide–GFP viruses? Within the primary infected APC, several aspects of cellular processing and presentation may impact the level of viral pMHC presentation. First, Vac:IA^b–peptide infections may create more 3K peptide available to be presented. It is possible that Vac:IA^b–peptide infection produces more IA^b–peptide fusion protein than Vac:peptide–GFP infection produces peptide–GFP fusion proteins. Second, the Vac:3K–GFP viruses produce a fusion protein which requires the 3K peptide to be cleaved and transported into the endosome/lysosome by cellular machinery before being loaded onto MHC molecules and trafficking to the cell surface. In contrast, Vac:IA^b–3K infection produces IA^{b}β–3K fusion proteins that can directly pair with endogenous IA^{b}α chains to form a complete pMHC complex and be transported to the cell surface (4). This may allow the same amount of 3K peptide created following Vac:IA^b–3K infections to be more efficiently displayed as a pMHC complex on the cell surface, compared with 3K peptide produced following Vac:3K–GFP infections. Third, the IA^b–peptide fusion protein has a linker between the peptide and the MHCβ chain. Although this linker is often cleaved in APCs that express the invariant chain, some cell surface-expressed viral pMHC may continue to have the peptide linked to the IA^{b}β chain (4). Having an MHC-linked peptide could allow the same peptide, if it is released from the MHC, to rebind the same MHC and, thus, extend the lifetime of the pMHC complex. All three mechanisms could result in a greater level of viral pMHC complex displayed on the cell surface.

Summary of the TCR–pMHC Confinement-Time Model for the Activation of CD4 T Cells. T-cell activation has been extensively studied in vitro and in vivo and the potency of pMHC ligands has been primarily ascribed to the $t_{1/2}$ or the K_D of the TCR–pMHC interaction. By studying pMHC ligands that have different K_D and binding kinetics, we and others have found that ligand potency measured in in vitro assays does not always follow a strict $t_{1/2}$ or K_D model of activation (2, 3). We found that for individual CD4 T cells, ligand potency followed the overall trend of both K_D- and $t_{1/2}$-based models. However, when we compared the activation profiles of multiple CD4 T cells (B3K506 and B3K508 T cells) with several defined pMHC ligands (3K and APL variants), neither model sufficed (2).

In regards to the K_D model of activation, B3K508 CD4 T cells are activated too well. For example, the B3K506 and B3K508 TCRs interact with the IA^b+3K complex with differing K_D (7 μM for the B3K506; 29 μM for the B3K508), and yet naïve B3K506 and B3K508 CD4 T cells proliferate and produce TNFα in response to similar titrating concentrations of soluble 3K peptide in vitro. In another example, the B3K506 TCR binds IA^b+P-1A (26 μM) with similar K_D as the B3K508 TCR binding to IA^b+3K (29 μM), and yet B3K506 CD4 T cells proliferate at an EC_{50} that is 23-fold less than B3K508 T cells. These and other previously tested 3K APLs indicated that the K_D of a TCR–pMHC interaction does not define the ligand potency.

Similarly, ligand potency measured using in vitro assays did not correlate with the $t_{1/2}$ because B3K506 CD4 T cells are activated too well. B3K506 CD4 T cells ($t_{1/2}$ = 0.9 s) and B3K508 CD4 T cells ($t_{1/2}$ = 2.2 s) proliferate and produce TNFα in vitro in response to similar concentrations of soluble 3K peptide and yet have different $t_{1/2}$. Additional discrepancies were observed when comparing other 3K APLs, including the demonstration that the P5R ligand is significantly less potent at activating B3K508 CD4 T cells than the 3K ligand is at activating B3K506 CD4 T cells, despite having a similar $t_{1/2}$ (0.7 and 0.9 s, respectively).

We consistently observed that the activating ligands for B3K506 T cells used fast on-rates to create a strong K_D and that this was compensating for short $t_{1/2}$. Vice versa, the B3K508 T cells engage IA^b+3K ligands with a longer $t_{1/2}$, which allows pMHC ligands with weaker K_D to be highly potent. Collectively, these findings suggested to us that the potency of a pMHC ligand is determined by an interplay between the on-rate and $t_{1/2}$ (or K_D and $t_{1/2}$) of the TCR–pMHC interactions, in a way that allows fast-kinetic ligands to have enhanced signaling properties.

In an attempt to reconcile how the interplay of K_D and binding kinetics influences T-cell activation, we analyzed our in vitro ligand-potency data within the context of several potential models. These included whether serial triggering or TCR–pMHC occupancy when TCR and pMHC are membrane-bound could explain our dataset; see SI text by Govern et al. (2) for a complete analysis of the tests, estimations, and assumptions used to convert the equilibrium affinity and binding kinetics of TCR–pMHC interactions measured in solution to those that are anchored onto membranes. These analyses indicated that ligand potency models based on K_D (receptor occupancy), $t_{1/2}$, or serial-triggering models did not fit our dataset.

Another model, TCR–pMHC confinement time, was found to best predict the activation of CD4 T cells in vitro. The confinement-time model is a TCR–pMHC kinetic model that incorporates rebinding: the ability of an individual receptor/ligand pair to associate, disassociate, and reassociate in a finite amount of time before complete disengagement (2, 3, 5). Although TCR–pMHC interactions are usually thought of as single binding events, TCR/ligand pairs with fast on-rates may be able to rebind (6), especially because they are bound on membranes where diffusivities are typically slower than in solution. TCR–pMHC rebinding would create an aggregate dwell time of interaction (the confinement time), t_a, assuming the rebindings occur faster than the TCR signaling-complex disassembles.

The t_a (aggregate dwell time or confinement time) depends on both the $t_{1/2}$, which determines the duration of any individual binding interaction, and the k_{on}, which determines how many times an individual TCR and pMHC rebind before diffusing away from each other. In addition, the t_a depends on a threshold on-rate for rebindings, k^*_{on}. TCR–pMHC pairs with on-rates faster than this threshold are predicted to rebind at least once. Further increases in the on-rate allow rebinding to occur more often than TCR–pMHC pairs with slower on-rates. The t_a has a qualitatively different dependence on the $t_{1/2}$ and k_{on} when on-rates are slow versus fast. When on-rates are fast relative to the membrane diffusion rates, pMHC binds and rebinds the same TCR many times reaching a quasiequilibrium before diffusing away. This causes the equilibrium affinity (a simple function of the k_{on} and $t_{1/2}$) to become the dominant factor that determines the t_a of the interaction. However, when on-rates are slow, rebinding does not occur and the t_a equals the $t_{1/2}$ of an individual TCR–pMHC engagement.

TCR–pMHC confinement-time models predict that ligand potency is dependent upon the aggregate dwell time of interaction and not just the $t_{1/2}$ of an individual TCR–pMHC engagement. In essence, the TCR–pMHC confinement-time model incorporates TCR–pMHC rebinding within a standard $t_{1/2}$ model.

Our TCR–pMHC t_a model was generated without empirically fitting the B3K506 or B3K508 CD4 T-cell activation data. The rebinding threshold, the only parameter in the model, was predicted to be ~60,000/(M × s), based on experimentally measured biophysical parameters. In comparing the model to the activation profiles of B3K506 and B3K508 CD4 T cells responding to strong-potency ligands, we found that 60,000/(M × s) is near the best fit for minimizing the variation in the aggregate $t_{1/2}$. Quite similarly, for medium-potency ligands, the best-fit threshold was found to be ~45,000/(M × s). The ability of the TCR–pMHC confinement-time model to predict the in vitro potency of CD4 T-cell ligands, in which there is a variance of k_{on}, k_{off}, and K_D, suggests the assumptions and underlying biophysical mechanisms are correct. Furthermore, direct evidence of rebinding has been observed between membrane-bound CD2 and CD58 using Fluorescence recovery after photobleaching (FRAP), as well as Src homology 2-containing proteins near the plasma membrane, indicating that fast-binding receptor ligand pairs can have significant increases in the duration of the bonds (7–9).

Statistical Analysis of Whether Antiviral CD4 T-Cell Responses in Vivo Correlate Best with the K_D, $t_{1/2}$, or t_a of the Viral pMHC–TCR Interaction. How well CD4 T-cell activation profiles generated using in vitro assays correlate with in vivo CD4 T-cell responses to viral infection is unclear. To elucidate whether antiviral CD4 T-cell burst size is predicted by specific biophysical parameters of the TCR–pMHC interaction, we compared the clonal burst size and maintenance of B3K508 and B3K506 T cells responding to each infection with the previously measured TCR–pMHC K_D, $t_{1/2}$, or calculated t_a. This allowed for three groups of T-cell responses to be compared based on whether the TCR–pMHC interaction has a similar K_D, $t_{1/2}$, or calculated t_a (Table S1) (2). The t_a was calculated using two values for the threshold on-rate for rebinding, k^*_{on} [k^*_{on} = 60,000/(M × s); and k^*_{on} = 45,000/(M × s)], because these values correspond to our theoretically derived value and our empirically derived, best-fit value for the threshold on-rate for rebinding (Table S1). Using different values of k^*_{on} models the uncertainties in different parameters that affect k^*_{on}, including the diffusivities of the TCR and the pMHC, and the conversion from SPR-measured k_{on} to k_{on} on the membrane. It is also a rough way of accounting for other factors that might increase or decrease the likelihood of rebinding, such as membrane motion; see Govern et al. for a complete description of the calculation (2).

We used three different statistical analyses to determine whether TCR–pMHC K_D, $t_{1/2}$, or calculated t_a best predicts CD4 T-cell responses in vivo. The first analysis, in the main text, involved analyzing groups of similar K_D, $t_{1/2}$, or calculated t_a for outliers. As a second analysis, we used a simple linear regression to determine how strongly the burst size is correlated with the different parameters. This method of analysis has been used previously to evaluate confinement-time models (10). The third analysis used a mutual information metric to allow for possible nonlinear relationships between the burst size and the kinetic parameters. Using all methods, we found that the calculated t_a was the best predictor of CD4 T cells responding to viral infections.

Using a linear regression analysis of the size of the T-cell response after infection with Vac:peptide–GFP viruses, we found an r^2 value for t_a [k^*_{on} = 60,000/(M × s)] to be 0.76 for the burst size and 0.75 during the maintenance phase, and for t_a [k^*_{on} = 45,000/(M × s)] to be 0.82 for the burst size and 0.85 during the maintenance phase (Fig. 5). In contrast, the r^2 values for $t_{1/2}$ are 0.34 for the burst size and 0.25 during the maintenance phase, whereas the r^2 values for K_A are 0.42 for the burst size and 0.55 during the maintenance phase. Thus, T-cell response correlates most strongly with t_a. The results for infection with Vac:IA^b–3K are similar but do not strongly discriminate between K_A and t_a models (Fig. S4).

In general, the relationship between burst size and the different kinetic parameters may be nonlinear (e.g., doubling t_a may more than double the burst size or it may less than double it). To analyze the data in way that allows for possible nonlinearities, we compared the mutual information between K_A, $t_{1/2}$, or t_a and the burst size, rather than the correlation coefficient as in the linear analysis. The mutual information between two variables is a measure of how well knowing one variable provides information about the value of the other (11). For example, if K_A were the only biophysical parameter that determines burst size, then we would expect knowing the value of K_A to enable us to predict the burst size accurately, except for some uncertainty that comes from other confounding factors and the intrinsic stochasticity of the T-cell response to stimulation. The correlation coefficient also measures how well knowing a parameter enables prediction of the response, but it forces linear predictions. In contrast, mutual information does not make an assumption about the functional relationship between variables (12).

To calculate mutual information, we binned the data according to the independent (K_A, $t_{1/2}$, or t_a) and log-transformed dependent (T-cell expansion) variables. Because the amount of data are limited, we chose three bins for each. We then calculated mutual information as:

$$I(X;Y) = \sum_{i=1}^{3}\sum_{j=1}^{3} p_{ij} \ln \frac{p_{ij}}{p_{i\text{-}}p_{\text{-}j}} \qquad \text{[S2]}$$

where $X = K_A$, $t_{1/2}$, or t_a; Y is the response; $p_{i\text{-}}$ is the fraction of data points that falls in the ith bin of the independent variable

(K_A, $t_{1/2}$, or t_a); $p_{\cdot j}$ is the fraction that falls in the jth bin of the dependent variable (the response); and p_{ij} is the fraction that falls in both the ith independent variable bin and the jth dependent variable bin. The parameters $p_{i\cdot}$, $p_{\cdot j}$, and p_{ij} summarize the data by describing how much of it falls in different ranges of the independent and dependent variables. Higher values of the mutual information $I(X;Y)$ correspond to noiseless relationships between X and Y, whereas scores that tend to 0 are statistically independent variables (12).

The best possible mutual information score for any of the independent variables is 0.64 nats, the entropy (self-information) of the response variable at this level of binning. The unit "nats" indicates that the logarithm in Eq. **S2** is a natural logarithm. This maximum score reflects the fact that there are only three possible values of the response at the level of our binning, so knowing the value of K_A, $t_{1/2}$, or t_a can decrease our uncertainty about the response, at most, by removing two possibilities for the bin in which it falls. For the response to Vac:peptide–GFP infections at day 7, the information contents of K_A, $t_{1/2}$, t_a [k^*_{on} = 45,000/(M × s)] and t_a [(k^*_{on} = 60,000/(M × s)] were 50%, 27%, 100%, and 100% of the maximum, respectively. Thus, t_a contains the maximal possible information at this level of binning. The results corroborate the conclusion that the confinement time is the best explanatory variable for the clonal burst size of CD4 T cells responding to vaccinia infections, although the significance of the metric is limited by the size of the datasets. Increasing or decreasing the number of bins resulted in too many data points falling in separate bins of the dependent or independent variable or too many data points falling in the same bin, compromising the statistics. However, for bin numbers in the range of 1–5, K_D or $t_{1/2}$ never provided more information about the response than the confinement time. For the response at 28 d to Vac:peptide–GFP infections, the results were similar: the information content of K_A, $t_{1/2}$, t_a [k^*_{on} = 45,000/(M × s)] and t_a [k^*_{on} = 60,000/(M × s)] were 50%, 27%, 100%, and 100% of the maximum, respectively. Collectively, using three different statistical tests that differ in the scale at which they analyze the data, and in their assumptions about linearity of the relationship between the kinetic variables and the response, t_a was found to be the best predictor of primary CD4 T-cell responses.

1. Huseby ES, Crawford F, White J, Marrack P, Kappler JW (2006) Interface-disrupting amino acids establish specificity between T cell receptors and complexes of major histocompatibility complex and peptide. *Nat Immunol* 7(11):1191–1199.
2. Govern CC, Paczosa MK, Chakraborty AK, Huseby ES (2010) Fast on-rates allow short dwell time ligands to activate T cells. *Proc Natl Acad Sci USA* 107(19):8724–8729.
3. Liu XQ, et al. (2002) Alternate interactions define the binding of peptides to the MHC molecule IA(b). *Proc Natl Acad Sci USA* 99:8820–8825.
4. Ignatowicz L, Winslow G, Bill J, Kappler J, Marrack P (1995) Cell surface expression of class II MHC proteins bound by a single peptide. *J Immunol* 154(8):3852–3862.
5. Valitutti S, Coombs D, Dupré L (2010) The space and time frames of T cell activation at the immunological synapse. *FEBS Lett* 584(24):4851–4857.
6. Dushek O, Das R, Coombs D (2009) A role for rebinding in rapid and reliable T cell responses to antigen. *PLOS Comput Biol* 5(11):e1000578.
7. Tolentino TP, et al. (2008) Measuring diffusion and binding kinetics by contact area FRAP. *Biophys J* 95(2):920–930.
8. Kaizuka Y, Douglass AD, Vardhana S, Dustin ML, Vale RD (2009) The coreceptor CD2 uses plasma membrane microdomains to transduce signals in T cells. *J Cell Biol* 185(3): 521–534.
9. Oh D, et al. (2012) Fast rebinding increases dwell time of Src homology 2 (SH2)-containing proteins near the plasma membrane. *Proc Natl Acad Sci USA* 109(35): 14024–14029.
10. Dushek O, et al. (2011) Antigen potency and maximal efficacy reveal a mechanism of efficient T cell activation. *Sci Signal* 4(176):ra39.
11. Cover TM, Thomas JA (2006) *Elements of Information Theory* (Wiley-Interscience, Hoboken, NJ), 2nd Ed.
12. Reshef DN, et al. (2011) Detecting novel associations in large data sets. *Science* 334(6062):1518–1524.

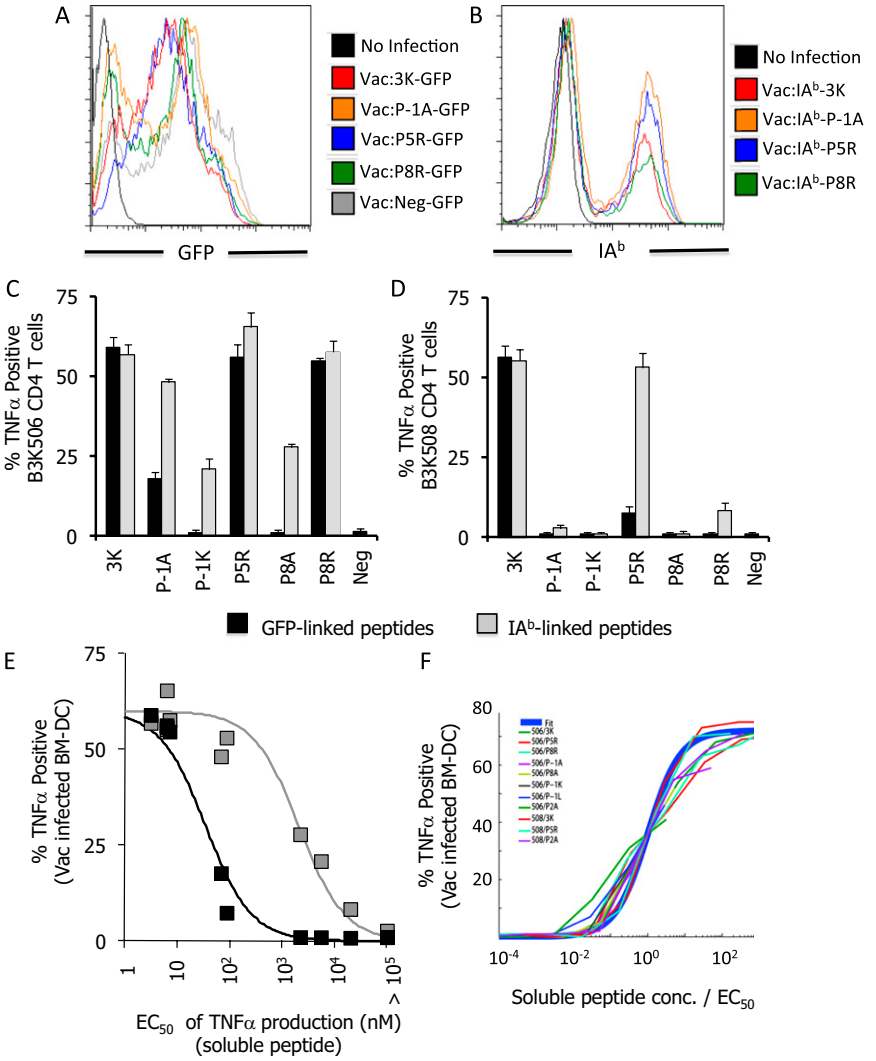

Fig. S1. BM-DCs infected with vaccinia viruses expressing 3K and 3K APLs fused to GFP or IA^b differentially activated naïve 3K-specific B3K506 and B3K508 CD4 T cells. (*A*) BM-DCs infected with Vac:peptide–GFP viruses express similar levels of GFP. (*B*) BM-DCs, differentiated from MHC class II-deficient mice that are infected with Vac:IA^b–peptide viruses, express similar levels of MHC class II. Naïve B3K506 T cells (*C*) or B3K508 T cells (*D*) were incubated with BM-DCs (differentiated from C57BL/6 mice) infected with Vac:peptide–GFP (black bars) or Vac:IA^b–peptide (gray bars) and analyzed for TNFα expression; 3K or 3K APL is listed on the *x* axis. Data are the average of three independent experiments. (*E*) The production of TNFα by naïve B3K506 and B3K508 T cells incubated with BM-DCs infected with Vac:peptide–GFP (black squares) and Vac:IA^b–peptide (gray squares) was compared with the concentration of soluble peptide that induces half-maximal TNFα production, i.e., the EC_{50} value (Table S1). The fit curves are described in *SI Materials and Methods*. (*F*) The parameters used in fitting viral potency are consistent with in vitro dose–response curves. T-cell dose–response curves (2) have a sigmoidal shape with respect to the logarithm of the peptide concentration. The fit is based on Eq. **S1** with measured EC_{50} values, treating peptide concentration as the independent variable. Fit parameters: r_{max} = 72%; n = 1.

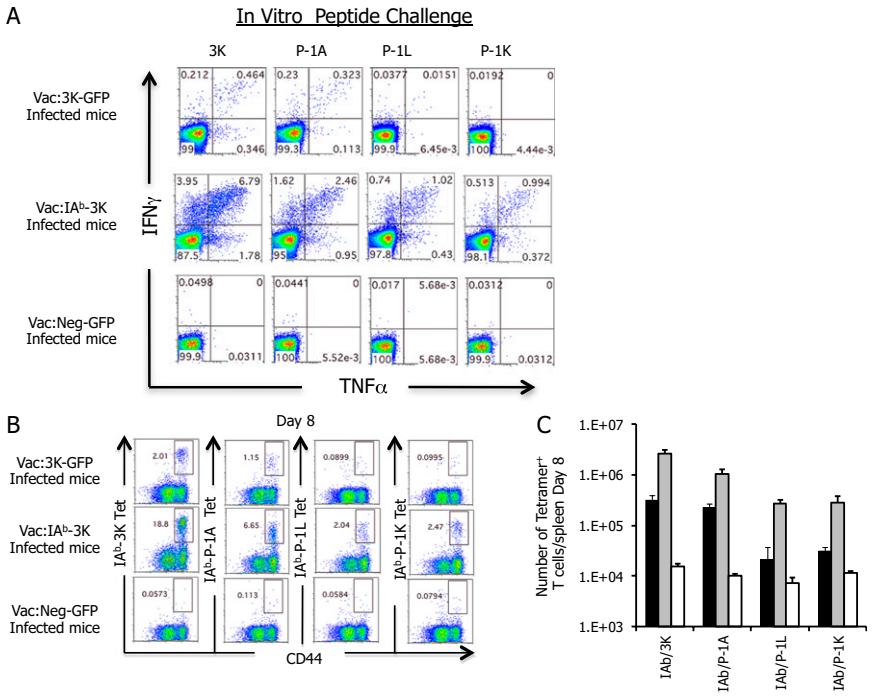

Fig. S2. Expansion of 3K-, P-1A–, P-1L–, and P-1K–reactive, IFNγ-producing and tetramer-positive CD4 T cells in the spleen of 506β mice 8 d postinfection. (*A*) Representative example of CD4 T cells from 506β mice infected with Vac:3K–GFP (top row), Vac:IA^b–3K (middle row), or Vac:Neg–GFP (bottom row) for the ability to produce IFNγ and TNFα following stimulation with 1 μg/mL 3K, P-1A, P-1L, or P-1K peptide. (*B*) CD4 T cells from 506β mice infected with Vac:3K–GFP (top row), Vac:IA^b–3K (middle row), or Vac:Neg–GFP (bottom row) were analyzed for the ability to be stained with IA^b–3K, –P-1A, –P-1L, or –P-1K tetramers. (*C*) Quantification of the total number of CD4 T cells per spleen that are stained with IA^b–3K, –P-1A, –P-1L, or –P-1K tetramer on day 8 following infection with Vac:3K–GFP (black bars), Vac:IA^b–3K (gray bars), or Vac:Neg–GFP (white bars). Data are the average of six total mice per group.

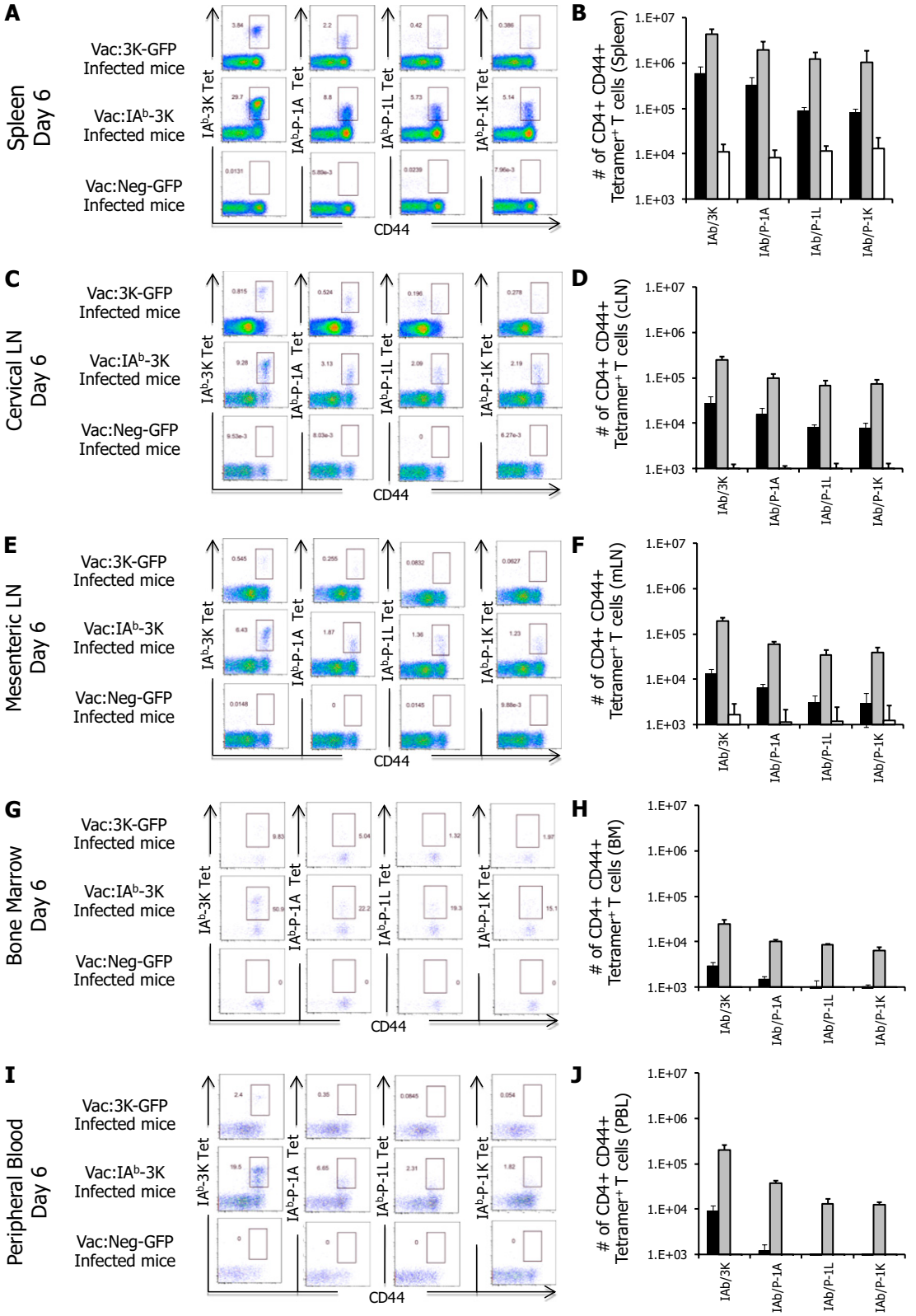

Fig. S3. CD4 T cells that are 3K, P-1A, P-1L, and P-1K tetramer-positive accumulate in the spleen and, to a lesser extent, in other secondary lymphoid organs on day 6 after vaccinia infection. (*A* and *B*) Mice (506β) were infected with Vac:3K–GFP (top row), Vac:IA^b–3K (middle row), or Vac:Neg–GFP (bottom row), and CD44+ CD4+ FACS-gated T cells isolated from the spleen of mice were stained with 1 μg/mL 3K, P-1A, P-1L, and P-1K tetramer (*A*) and quantified (*B*). For quantification, Vac:3K–GFP–infected mice are black solid bars, Vac:IA^b–3K–infected mice are gray solid bars, and Vac:Neg–GFP–infected mice are white solid bars. These same mice were analyzed for 3K, P-1A, P-1L, and P-1K tetramer-positive CD44+ CD4+ gated T cells present in the cervical lymph nodes (*C* and *D*), mesenteric lymph nodes (*E* and *F*), bone marrow (*G* and *H*), and peripheral blood (*I* and *J*). For blood quantification, it was assumed a 20-g mouse has 1.5 mL of blood. Data are representative of average of four mice per group.

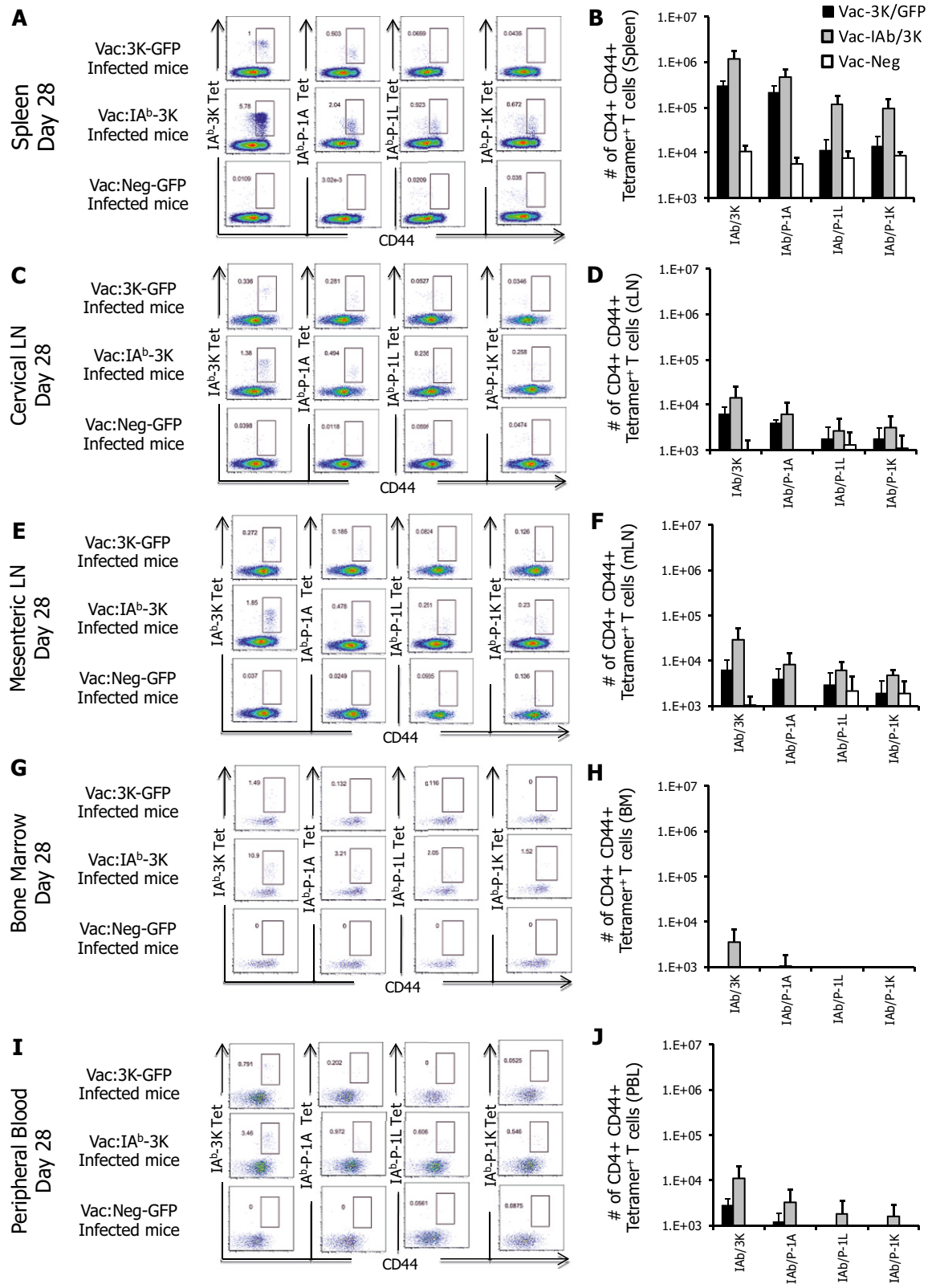

Fig. S4. CD4 T cells that are 3K, P-1A, P-1L, and P-1K tetramer-positive accumulate in the spleen and, to a lesser extent, in other secondary lymphoid organs on day 28 after vaccinia infection. (*A* and *B*) Mice (506β) were infected with Vac:3K–GFP (top row), Vac:IA^b–3K (middle row), or Vac:Neg–GFP (bottom row), and CD44+ CD4+ FACS-gated T cells isolated from the spleen of mice were stained with 1 μg/mL 3K-, P-1A, P-1L, and P-1K tetramer (*A*) and quantified (*B*). For quantification, Vac:3K–GFP–infected mice are black solid bars, Vac:IA^b–3K–infected mice are gray solid bars, and Vac:Neg–GFP–infected mice are white solid bars. These same mice were analyzed for 3K, P-1A, P-1L, and P-1K tetramer-positive CD44+ CD4+ gated T cells present in the cervical lymph nodes (*C* and *D*), mesenteric lymph nodes (*E* and *F*), bone marrow (*G* and *H*), and peripheral blood (*I* and *J*). For blood quantification, it was assumed a 20-g mouse has 1.5 mL of blood. Data are representative of average of five mice per group.

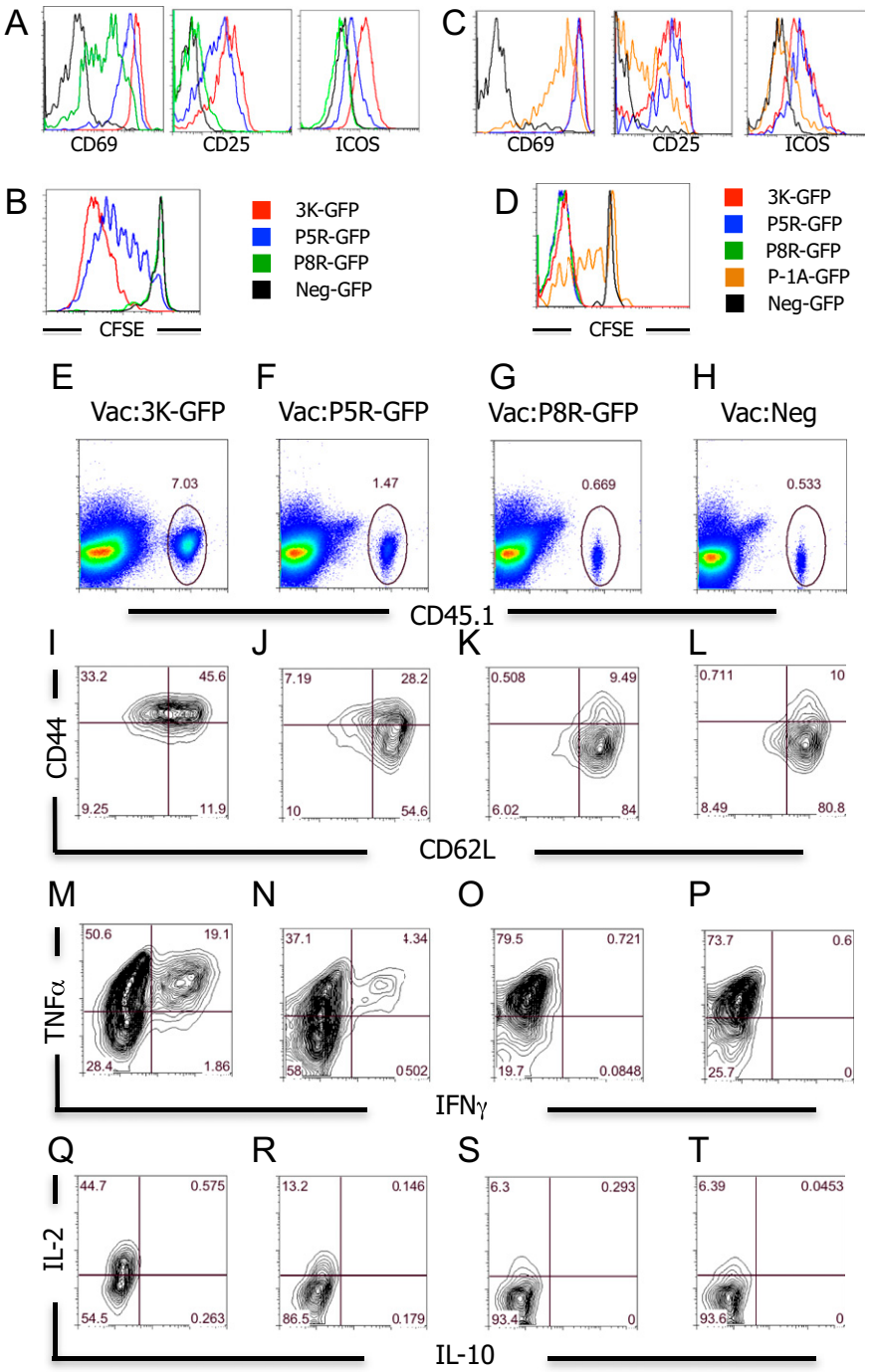

Fig. S5. Infection of mice with Vac:peptide–GFP virus induces three categories of early CD4 T-cell response: weak-potency ligands induce the expression of T-cell surface markers associated with activation but fail to induce proliferation; medium-potency ligands induce the expression of activation markers at an intermediate level and modest proliferation; strong-potency ligands induce robust expression of activation markers and T-cell proliferation. (*A*) B6.CD45.1$^+$ B3K508 T cells (1×10^6) were transferred into C57BL/6 mice and infected with Vac:3K–GFP (strong potency, red), Vac:P5R–GFP (medium potency, blue), Vac:P8R–GFP (weak potency, green), or Vac:Null–GFP (null potency, black) virus. B3K508 CD4 T cells were analyzed 18 h postinfection for the expression of CD69 or 48 h postinfection for the expression of CD25 and ICOS. (*B*) B3K508 T cells labeled with CFSE were analyzed for cellular proliferation 3 d after infection. Data are representative of six mice per group. (*C*) B6.CD45.1$^+$ B3K506 T cells (1×10^6) were transferred into C57BL/6 mice and infected with Vac:3K–GFP (strong potency, red), Vac:P5R–GFP (strong potency, blue), Vac:P8R–GFP (strong potency, green), Vac:P-1A–GFP (medium potency, orange), or Vac:Null–GFP (null potency, black) virus. B3K506 CD4 T cells were analyzed 18 h postinfection for the expression of CD69 or after 48 h for the expression of CD25 and ICOS. (*D*) B3K506 T cells labeled with CFSE were analyzed for cellular proliferation 3 d after infection. Data are representative of six mice per group. (*E*–*T*) Three days after Vac:peptide–GFP virus infection carrying weak-, medium-, and strong-potency ligands, B3K508 CD4 T cells show distinct changes in the activation markers, CD44 and CD62L, and have a differential ability to produce IFNγ. B6.CD45.1$^+$ B3K508 T cells (1×10^6) were transferred into C57BL/6 mice and infected with Vac:3K–GFP (strong potency, column 1) (*E*), Vac:P5R–GFP (medium potency, column 2) (*F*), Vac:P8R–GFP (weak potency, column 3) (*G*), or Vac:Null–GFP (null potency, column 4) (*H*) virus. Seventy-two hours postinfection, B3K508 CD4 T cells were identified using the congenic marker, CD45.1, and analyzed for the expression of CD44 and CD62L (*I*–*L*) or for the ability to produce IFNγ and TNFα (*M*–*P*) or IL-2 and IL-10 (*Q*–*T*). Data are representative of four mice per group.

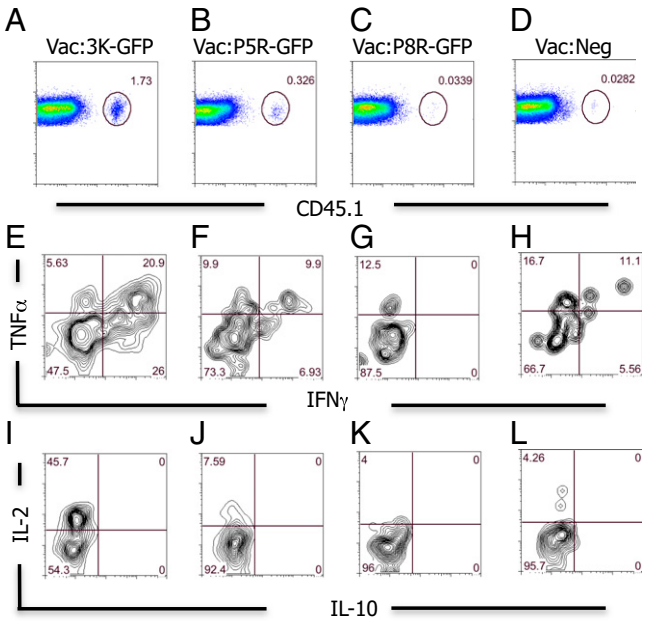

Fig. S6. Seven days after Vac:peptide–GFP virus infection, activated B3K508 CD4 T cells are strong producers of IFNγ, TNFα, and IL-2 when the virus carries a strong potency ligand. B6.CD45.1$^+$ B3K508 T cells (1×10^5) were transferred into C57BL/6 mice and infected with Vac:3K–GFP (strong potency, column 1) (*A*), Vac:P5R–GFP (medium potency, column 2) (*B*), Vac:P8R–GFP (weak potency, column 3) (*C*), or Vac:Null–GFP (null potency, column 4) (*D*) virus. Seven days postinfection, B3K508 CD4 T cells were identified using the congenic marker, CD45.1, and analyzed for the ability to produce IFNγ and TNFα (*E*–H) or IL-2 and IL-10 (*I*–*L*). Data are representative of six mice per group.

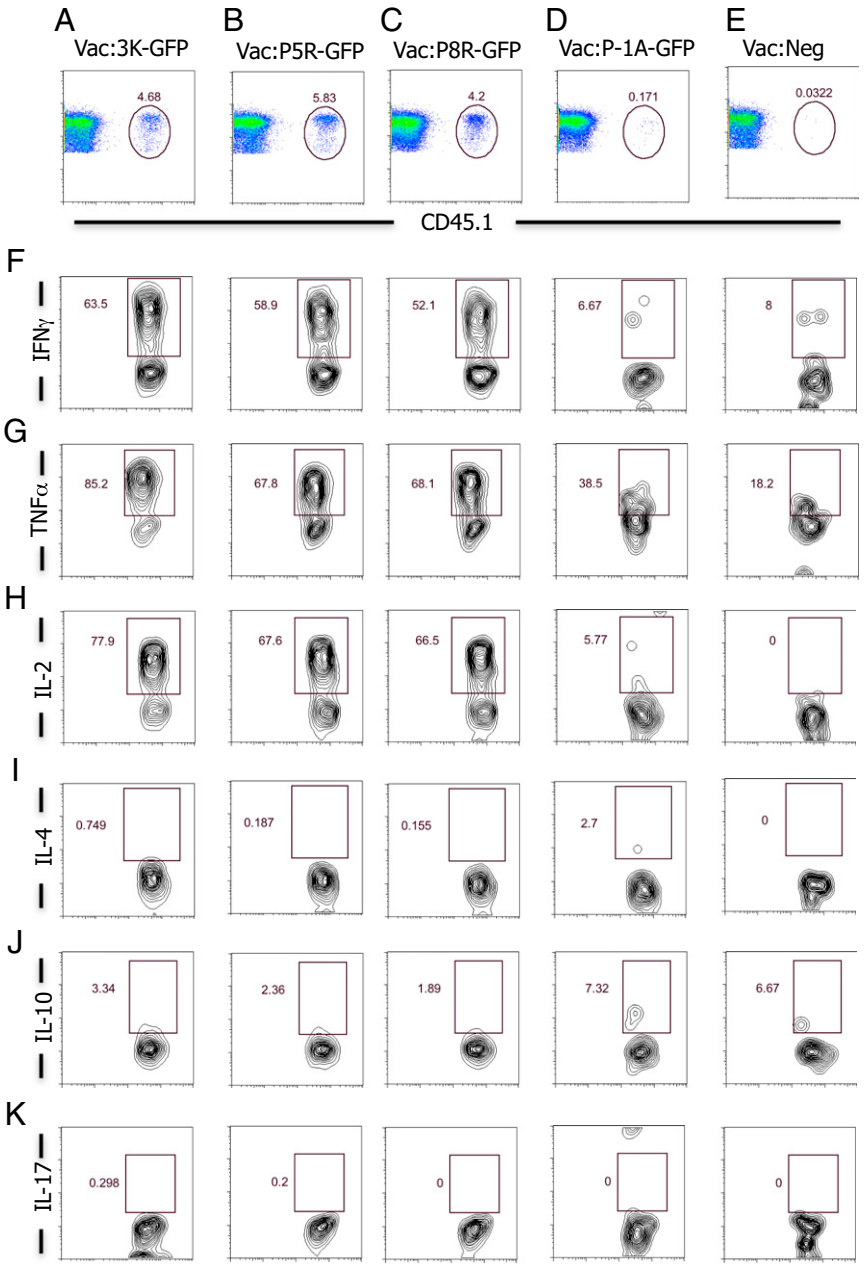

Fig. S7. Seven days after Vac:peptide–GFP virus infection, activated B3K506 CD4 T cells are strong producers of IFNγ, TNFα, and IL-2 when the virus carries a strong potency ligand. B6.CD45.1$^+$ B3K506 T cells (1×10^5) were transferred into C57BL/6 mice and infected with Vac:3K–GFP (strong potency, column 1) (*A*), Vac:P5R–GFP (strong potency, column 2) (*B*), Vac:P8R–GFP (strong potency, column 3) (*C*), Vac:P-1A–GFP (medium potency, column 4) (*D*), or Vac:Null–GFP (null potency, column 5) (*E*) virus. Seven days postinfection, B3K506 CD4 T cells were identified using the congenic marker, CD45.1, and analyzed for the ability to produce IFNγ (row *F*), TNFα (row *G*), IL-2 (row *H*), IL-4 (row *I*), IL-10 (row *J*), or IL-17 (row *K*). Data are representative of four mice per group.

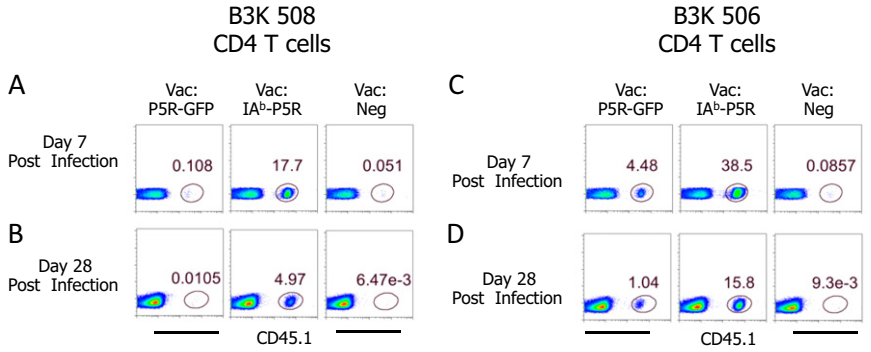

Fig. S8. Infection of mice with Vac:IA^b-linked peptides allows medium-potency ligands to induce massive expansion and maintenance CD4 T cells. (*A* and *B*) CD45.1$^+$ B3K508 CD4 T cells (1×10^5) were transferred into C57BL/6 mice and infected with the medium potency peptide, P5R, fused to GFP (Vac:P5R–GFP, column 1), IA^b (Vac:IA^b–P5R, column 2), or Vac:Neg (column 3). At 7 d (*A*) or 28 d (*B*) postinfection, the B3K508 CD4 T cells were identified from spleen cells of infected mice as CD8^{neg}, MHC CL2^{neg}, Thy1.2$^+$, CD4$^+$, CD45.1$^+$ cells. FACS plots are shown comparing endogenous CD4 T cells (CD45.1^{neg}) with B3K508 CD4 T cells (CD45.1$^+$). Note the massive increase of B3K508 T cells in the spleen of infected mice following Vac:IA^b–P5R infections compared with Vac:P5R–GFP infections on both day 7 and day 28. Data are representative of six mice per group. (*C* and *D*) As a control for the P5R viruses, 1×10^5 CD45.1$^+$ B3K506 CD4 T cells were transferred into C57BL/6 mice and infected with the same Vac:P5R–GFP (column 1), Vac:IA^b–P5R (column 2), or Vac:Neg (column 3) virus. The P5R peptide is a strong potency ligand for the B3K506 T cells. Note the increase in expansion (day 7) and maintenance (day 28) of B3K506 T cells responding to Vac:P5R–GFP infection, compared with B3K508 T cells responding to the same Vac:P5R–GFP virus infection. Data are representative of six mice per group.

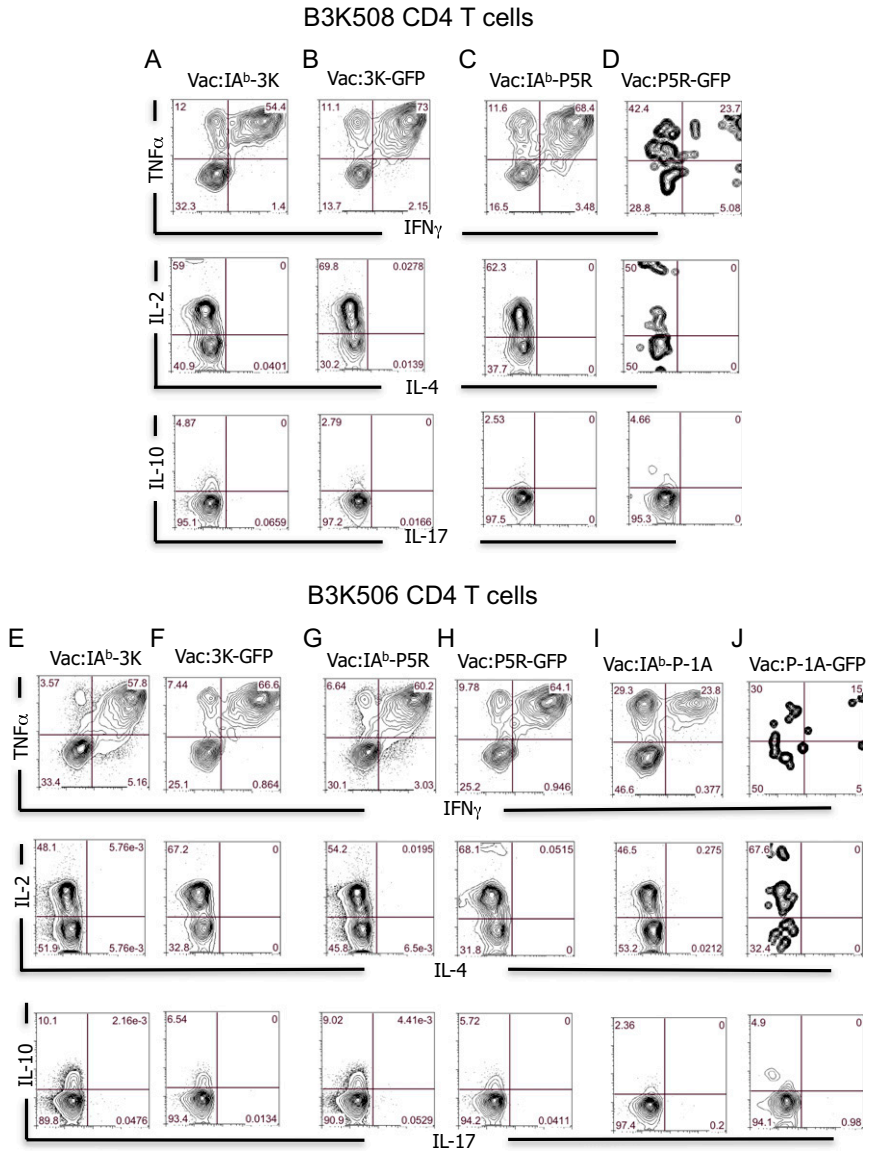

Fig. S9. CD4 T cells responding to Vac:IA^b-linked peptide infections carrying medium-potency ligands are strong producers of IFNγ, TNFα, and IL-2. (*A–D*) CD45.1$^+$ B3K508 CD4 T cells (1×10^5) were transferred into C57BL/6 mice. Recipient mice were infected with either the strong-potency peptide, 3K, fused to IA^b (Vac:IA^b–3K, column 1) (*A*) or fused to GFP (Vac:3K–GFP, column 2) (*B*), or the medium-potency peptide, P5R, fused to IA^b (Vac:IA^b–P5R, column 3) (*C*) or fused to GFP (Vac:P5R–GFP, column 4) (*D*). Seven days after infection, CD45.1$^+$ B3K508 CD4 T cells were analyzed for the ability to produce IFNγ and TNFα (row 1), IL-4 and IL-2 (row 2), and IL-17A and IL-10 (row 3). Note the strong IFNγ production by B3K508 CD4 T cells responding to Vac:IA^b–P5R infection. Data are representative of four mice per group. (*E–J*) CD45.1$^+$ B3K506 CD4 T cells (1×10^5) were transferred into C57BL/6 mice. Recipient mice were infected with either the strong-potency peptide, 3K, fused to IA^b (Vac:IA^b–3K, column 1) (*E*) or fused to GFP (Vac:3K–GFP, column 2) (*F*), the strong-potency peptide, P5R, fused to IA^b (Vac:IA^b–P5R, column 3) (*G*) or fused to GFP (Vac:P5R–GFP, column 4) (*H*), or the medium potency peptide, P-1A, fused to IA^b (Vac:IA^b–P-1A, column 5) (*I*) or fused to GFP (Vac:P-1A–GFP, column 6) (*J*). Seven days postinfection, CD45.1$^+$ B3K506 CD4 T cells were analyzed for the ability to produce IFNγ and TNFα (row 1), IL-4 and IL-2 (row 2), and IL-17A and IL-10 (row 3). Note the strong IFNγ production by B3K506 CD4 T cells responding to Vac:IA^b–P-1A infection. Data are representative of four mice per group.

Table S1. TCR-pMHC–binding parameters and T-cell expansion size following vaccinia infections

TCR	IA^b + 3K APL	K_D (μM)	k_a [1/(s × M)]	k_d (1/s)	$t_{1/2}$ (s)	t_a*	t_a**	TNFα EC_{50} (nM)	Prolif. EC_{50} (nM)	No. of T cells on D7 Vac:GFP	SD	No. of T cells on D7 Vac:IA^b	SD	No. of T cells on D28 Vac:GFP	SD	No. of T cells on D28 Vac:IA^b	SD
B3K506	WT	7	101,918	0.7	0.9	3.1	2.7	3.1	0.2	414,218	242,334	5,590,687	3,045,605	303,437	56,682	2,884,693	741,567
B3K506	P-1A	26	101,731	2.6	0.3	0.9	0.7	68	9	3,314	1,715	2,561,640	1,085,543	2,963	1,428	694,038	230,595
B3K506	P5R	11	74,654	0.8	0.9	2.3	1.9	6	0.2	422,836	182,084	4,216,339	2,073,190	273,105	73,719	2,647,031	919,696
B3K506	P8R	13	64,318	0.8	0.8	2.1	1.8	7	0.3	319,989	144,777	4,082,395	1,808,778	225,663	41,534	2,911,135	583,145
B3K508	WT	29	10,887	0.3	2.2	2.8	2.8	6	0.4	299,249	163,077	4,189,068	1,390,348	146,340	45,593	1,688,821	597,863
B3K508	P-1A	>550	ND	ND	ND	0.1	0.1	$>10^4$	10,000	1,912	733	5,579	4,227	876	717	1,539	765
B3K508	P5R	93	11,048	1.0	0.7	0.9	0.8	87	15	14,277	5,193	2,028,295	631,288	2,211	1,150	824,807	195,536
B3K508	P8R	>550	ND	ND	ND	0.1	0.1	20,000	980	2,853	2,371	12,657	3,766	731	802	7,594	2,141

K_D, k_a, k_d, $t_{1/2}$, t_a*, t_a**, and TNFα EC_{50} and proliferation (prolif.) EC_{50} were reported in ref. 2. t_a* is based on k_{on}* = 45,000 $\mu m^2/s$; t_a** is based k_{on}* = 60,000 $\mu m^2/s$.